Quaternary Science Advances 12 (2023) 100109

Contents lists available at ScienceDirect

Quaternary Science Advances

journal homepage: www.sciencedirect.com/journal/quaternary-science-advances

Chronology and climate of the Last Glacial Maximum and the subsequent deglaciation in the northern Medicine Bow Mountains, Wyoming, USA

Eric M. Leonard [a,*], Benjamin J.C. Laabs [b], Shaun A. Marcott [c], Edward E. Crawford [a], Benjamin T. Mackall [a], Daniel E. Ibarra [d], Matthew B. Osman [e], Mitchell A. Plummer [f], Marc W. Caffee [g]

[a] Department of Geology, Colorado College, Colorado Springs, CO, 80903, USA
[b] Department of Earth, Environmental and Geospatial Sciences, North Dakota State University, Fargo, ND, 58108-6050, USA
[c] Department of Geoscience, University of Wisconsin, Madison, WI, 53706-1692, USA
[d] Department of Earth, Environmental and Planetary Science, The Institute at Brown for Environment and Society, Brown University, Providence, RI, 02912, USA
[e] Department of Geography, University of Cambridge, Cambridge, CB2 3EN, UK
[f] Idaho National Laboratory, P.O. Box 1625, Idaho Falls, ID, 83415-2107, USA
[g] Department of Physics and Astronomy and Department of Earth, Atmospheric, and Planetary Science, Purdue University, 525 Northwestern Ave, West Lafayette, IN, 47907-2036, USA

ARTICLE INFO

Keywords:
Last Glacial Maximum
Deglaciation
Paleoclimate
Cosmogenic surface-exposure dating
Glacier modeling
Wyoming

ABSTRACT

A combination of ^{10}Be surface-exposure dating of glacially transported boulders and glacially polished bedrock, and numerical modeling of the ~600 km^2 Late Pleistocene icefield complex in the northern Medicine Bow Mountains of Wyoming, USA, constrains the timing and climate forcing of the local last glacial maximum (LLGM) and the subsequent deglaciation in the range. The chronology reported here indicates initial recession of the ~100 km^2 Libby Creek glacier on the east side of the complex from its terminal moraine at 20.7 ± 2.8 ka, followed by length reduction of 38% by 18.0 ± 0.8 ka and 75% by 14.7 ± 0.4 ka. By 14.2 ± 0.3 ka, the icefield had nearly completely disappeared although there is evidence of two subsequent standstills or minor readvances at ~11.5 ± 0.5 ka and ~10.5 ± 0.3 ka. Results of numerical glacier-modeling experiments suggest that the LLGM was associated with temperatures 6.0 °C colder than present with an uncertainty of about ±1.7 °C, assuming no change from modern precipitation. If precipitation differed at the LLGM, over a range from half to twice modern, the temperature depression necessary to sustain the icefield complex could have been as much as 8.0 ± 1.7 °C or as little as 3.1 ± 1.7 °C respectively. As most available proxies and climate-model output suggest mildly decreased precipitation at the LLGM, a temperature depression of somewhat more than 6.0 °C is the most likely scenario. Model experiments further suggest that nearly complete deglaciation by 14.2 ± 0.3 ka involved only a ~1.7 °C rise from LLGM temperature, assuming no change in precipitation. The sensitivity of the icefield complex to such limited warming reflects its plateau-like hypsometry, which makes it particularly sensitive to changing equilibrium-line altitude. While the precise chronology of deglaciation remains open to interpretation, most of the ice loss preceded the North Atlantic Bølling-Allerød interval (~14.7–12.9 ka), suggesting that global atmospheric CO_2 and rising summer insolation were the dominant forcings of ice retreat.

1. Introduction

The termination of the last glaciation marks the most recent period of major global-scale warming. An understanding of the timing, nature, and rates of climate change involved during and following the Last Glacial Maximum (LGM, 26.5–19.0 ka; Clark et al., 2009) is critical to understanding the operation of the climate system and its response to different forcings, and ultimately to understanding how the climate system is likely to respond to future forcing (Tierney et al., 2020). Much is known about the timing and character of events through this period in some parts of the world. This is particularly true in regions with abundant deep-sea sediment-core or ice-core records, including some oceanic regions such as the North Atlantic Ocean, as well as Greenland and portions of Antarctica. By contrast, in many continental settings, where

* Corresponding author.
E-mail address: eleonard@coloradocollege.edu (E.M. Leonard).

https://doi.org/10.1016/j.qsa.2023.100109
Received 30 March 2023; Received in revised form 26 July 2023; Accepted 27 July 2023
Available online 2 August 2023

proxy records tend to be discontinuous and are often difficult to date and interpret, understanding of the local timing and character of the LGM and deglaciation is much less complete. Consequently, it has been difficult to establish a global overview of the period, impeding development of a full understanding of climate forcings.

Alpine glaciers provide some of the clearest evidence of past and present climate changes. With their sensitive, and generally rapid, response to climate, and the wide-spread occurrence and high degree of preservation of deposits from the last glaciation, they offer a potential for detailed reconstructions of the timing and character of climate changes during and following the LGM. Glacial deposits in the Rocky Mountain region of the western United States (Fig. 1, insert) have such potential. During the last glaciation alpine glaciers were present along almost the entire latitudinal range of the U.S. Rocky Mountains. Both climate models and available non-glacial proxy studies suggest that at the LGM temperature was depressed non-uniformly across the region, with decreasing temperature depression southward away from the margins of the Laurentide and Cordilleran ice sheets, and that LGM precipitation was likely lower than present in the northern portion of the Rocky Mountain region and higher than present in the southern portion (e.g. COHMAP Members, 1988; Thompson et al., 1993; Kutzbach et al., 1998; Bartlein and Hostetler, 2004; Oster et al., 2015, 2020; Lorenz et al., 2016; Ibarra et al., 2018; Morrill et al., 2018; Osman et al., 2021; PMIP3— https://pmip3.lsce.ipsl.fr [last accessed 2022-11-8]). The patterns, timing, and forcing of climate following the LGM in the region and across western North America are topics of ongoing research and refinement (Lora et al., 2016; Shuman and Serravezza, 2017; Hudson et al., 2019; Lora and Ibarra, 2019; Palacios et al., 2020). An understanding of the climate that sustained Rocky Mountain glaciers at the LGM and forced their subsequent recession can provide insight into regional climate evolution and its spatial variability, both supplementing, and allowing assessment of, inferences made based on climate models and other proxy records. These potential contributions of Rocky Mountain paleoglaciology to understanding of regional paleoclimate depend on the ability to date accurately the timing of the individual glacier maximum stands and the pacing of their subsequent recession, and to make reliable inferences about the climate necessary to sustain the glaciers at their maximum extents and to force deglaciation.

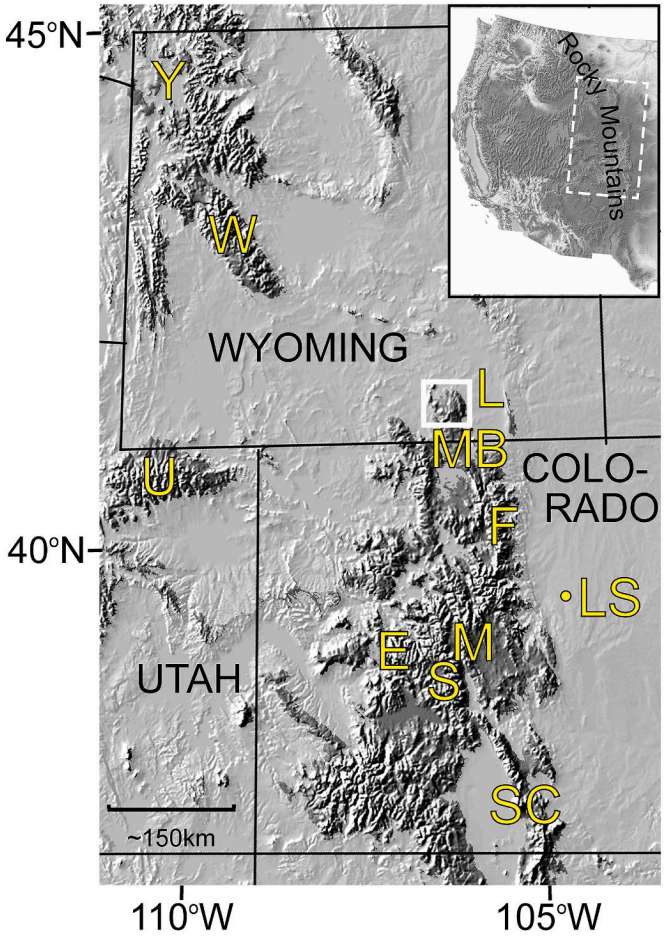

Fig. 1. Location map of Wyoming, Colorado and a portion of Utah, showing northern Medicine Bow Mountains study area (white box) and other sites mentioned in text. W – Wind River Range; L – Laramie Basin; MB – Medicine Bow Mountains; F – Colorado Front Range; LS – Lamb Springs archaeological site; M – Mosquito Range; S – Sawatch Range; E – Elk Mountains; SC – Sangre de Cristo Mountains. Yellowstone Plateau (Y) and Uinta Mountains (U) are also shown for reference. Insert map shows the western United States, with main map outlined with dashed line.

In recent decades understanding of the chronology of the last glacial maximum and subsequent deglaciation in the Rocky Mountains has improved with the application of surface-exposure dating of glacial features, primarily using the cosmogenic radionuclide ^{10}Be (see reviews by Leonard et al., 2017a; Laabs et al., 2020). In some areas of the Rocky Mountains, primarily in Utah and Colorado (Fig. 1), numerical modeling of paleoglaciers has put constraints of the character of local climate during the last glacial maximum (Laabs et al., 2006; Refsnider et al., 2008; Ward et al., 2009; Brugger, 2010; Dühnforth and Anderson, 2011; Birkel et al., 2012; Schweinsberg et al., 2016; Leonard et al., 2017a, 2017b, 2023,b; Quirk et al., 2018, 2020, 2022; Brugger et al., 2019a, 2019b, 2021). Five of these studies, all in Colorado, have also attempted to model climate forcing through the full post-LGM deglaciation interval (Ward et al., 2009; Dühnforth and Anderson, 2011; Schweinsberg et al., 2016; Leonard et al., 2017a, 2017b).

In this study we examine the evolution of a small late Pleistocene icefield complex in the northern Medicine Bow Mountains of southern Wyoming (Fig. 1). Our aims are twofold: first, to establish an accurate and detailed chronology of its changing extent from the time of the local last glacial maximum until ice disappeared completely from the area and, second, to derive quantitative estimates of regional climate that sustained the complex at its last glacial maximum extent and forced its subsequent recession. To do this, we use ^{10}Be surface-exposure dating of glacially transported boulders and glacially scoured bedrock to date the changing extent of the icefield, along with numerical modeling of paleoglacier energy and mass balance and ice flow to constrain the magnitude and character of climate changes associated with this changing ice extent. This is the first study to couple a full deglaciation chronology with numerical glacier modeling in the Rocky Mountain region outside of Colorado.

Here we use the term “Last Glacial Maximum” (or “LGM”) to refer to the global interval ~26.5–19.0 ka (Clark et al., 2009) during which most mountain glaciers and ice sheets reached their maximum extents of the last Pleistocene glaciation, and eustatic sea level was at a minimum. We use the term “local last glacial maximum (or “LLGM”) to refer to the maximum stand of an individual glacier during Marine Oxygen Isotope Stage 2 (29.0–14.0 ka—Lisiecki and Raymo, 2005), whether it occurred during the global LGM interval or not.

2. Study area

The Medicine Bow Mountains are the easternmost high range of the Rocky Mountains in southern Wyoming and northern Colorado (Fig. 1). The range extends about 140 km NNW-to-SSE, at its southern end adjoining the Colorado Front Range. The northern and southern ends of the range, which exceed 3600 m altitude in the north and 3900 m in the south, were extensively glaciated in the Late Pleistocene, and contain areas of high-relief alpine topography. Between these two areas, particularly in southernmost Wyoming, the range consists primarily of a rolling upland, nearly all below 3000 m, without alpine topography, which appears not to have been glaciated during the Pleistocene.

The northern glaciated portion of the range is the focus of this study (Fig. 2). In that area the range consists of an upland, largely above 3000 m, but incised by canyons several hundred meters deep. Standing above the center of this upland is the Snowy Range, a 12 km-long NE-SW-trending ridge generally at 3350–3650 m altitude, with a maximum altitude of 3661 m. The broad upland below the Snowy Range is bounded on its western, northern, and eastern sides by slopes extending down to surrounding basins, typically below 2500 m. The southern margin of the plateau is less clear, merging into somewhat lower terrain toward the Wyoming-Colorado border.

2.1. Bedrock geology

The central portion of the northern Medicine Bow Mountains, including nearly all of the area glaciated during the late Pleistocene, consists of Precambrian metasedimentary, metavolcanic and igneous rocks of both Archean and Proterozoic ages (Karlstrom et al., 1983; Houston and Karlstrom, 1992; Sutherland and Hausel, 2004). The highest portions of the range are underlain by Paleoproterozoic Medicine Peak Quartzite, a whitish rock whose appearance gave the Snowy Range its name. Along the eastern and northern margins of the range, Phanerozoic sedimentary rocks occur in both fault and depositional contact with the Precambrian rocks. Structures bounding the range and separating it from adjacent basins are primarily Laramide (latest Cretaceous-to-Eocene) in age. The eastern and northeastern margins of the range are characterized by thrust faults of that age juxtaposing the Precambrian and Phanerozoic rocks (Blackstone, 1987; Houston and Karlstrom, 1992). Houston and Karlstrom (1992) also cite evidence of later Neogene faulting, particularly in the western portion of the range.

2.2. Glaciation

The Snowy Range and the surrounding lower-relief terrain were glaciated multiple times during the Pleistocene, with a small (~600 km^2) icefield-outlet glacier complex occupying the high spine of the range, the surrounding plateau upland, and the valleys incised into it (Atwood, 1937; Mears, 2001). This complex, here termed the Northern Medicine Bow Icefield Complex, particularly its southeastern quadrant in the Libby and French Creek drainages (Fig. 2), is the subject of this study. At their last glacial maximum extent glaciers in Libby Creek drainage had an area of ~100 km^2, extending approximately 14 km eastward from broad snowfields occupying the plateau upland (locally referred to as the "Libby Flats") at the base of the Snowy Range at about 3300–3400 masl, to a terminal moraine complex just upvalley from the town of Centennial, Wyoming, reaching a terminal altitude of ~2575 masl. LLGM glaciers in the French Creek drainage had an area of ~60 km^2, extending approximately 16 km southward and southwestward from high snowfields contiguous with those of the Libby drainage, spanning a very similar elevation range. In Libby Creek valley, an extensive terminal moraine complex from the last glaciation is preserved over ~1 km of valley floor. A similar complex in the French Creek drainage is somewhat less clearly defined.

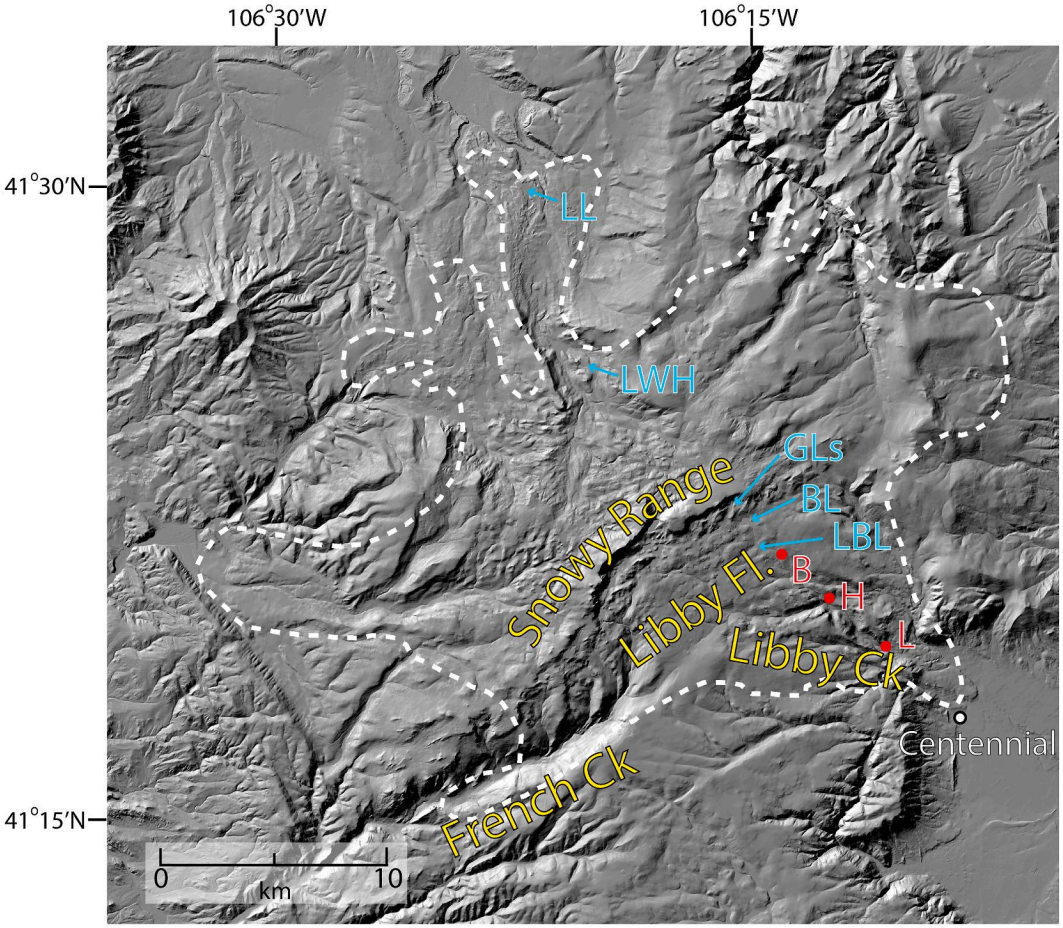

Fig. 2. Study area map of the northern Medicine Bow Mountains showing geographical features and study sites mentioned in text. LL – Long Lake; LWHP – Lower Windy Hill Pond; GLs – West and East Glacier Lakes; BL – Brooklyn Lake; LBL – Little Brooklyn Lake. Red circles are snow-survey localities utilized in model validation studies. B – Brooklyn Lake SNOTEL; H – Hairpin Turn snow course; L – Libby Lodge snow course. Dashed white line is the approximate limit of glacial till mapped by Mears (2001) and includes areas mapped as deposits from both the last and penultimate glaciations. (For interpretation of the references to colour in this figure legend, the reader is referred to the Web version of this article.)

Currently there are no glaciers in the northern Medicine Bow Mountains, and no permanent snowfields are indicated on USGS topographic maps. Examination of aerial photographs taken over the last several decades indicates that numerous small snowfields along the southeastern side of the Snowy Range last through the summer melt season in most years.

2.3. Climate

Modern climate in the northern Medicine Bow Mountains is strongly continental with relatively low precipitation and large diurnal and seasonal temperature variations. Meteorological data are available for several sites within or close to the southeastern sector of the Late Pleistocene icefield, the focus of this study. The Centennial 1 NE met station, at ~2480 m (Fig. 2—https://wrcc.dri.edu/cgi-bin/cliMAIN.pl?wy1610), at the eastern margin of the range, about 15 km east of range crest, has operated intermittently since 1899 CE, and generally continuously from 1948 CE until 2004 CE, except 1968–1977 CE. At higher elevation, data are available from a SNOTEL (SNOwpackTELemetry) station that has operated since 1981 CE near Brooklyn Lake at about 3120 m (Fig. 2—https://wcc.sc.egov.usda.gov/nwcc/site?sitenum=367), and from nearby US Forest Service meteorological stations at Brooklyn Lake (3182 m—USS0006H13S) and at still higher (~3280 m) West Glacier Lake (Fig. 2—https://www.fs.usda.gov/rmrs/experimental-forests-and-ranges/glees-glacier-lakes-ecosystem-experiments-site) where data have been collected since 1989 CE.

There is a strong altitudinal gradient in precipitation on the eastern side of the range, with mean annual precipitation of 355 mm at Centennial (1981–2007 CE—https://wrcc.dri.edu/cgi-bin/cliMAIN.pl?wy1610) and 897 mm at Brooklyn Lake SNOTEL (1981–2010 CE—https://wcc.sc.egov.usda.gov/nwcc/site?sitenum=367). At Centennial precipitation is fairly evenly distributed through the year with a weak summer maximum and a weak minimum in late fall and early winter. At the higher altitude Brooklyn Lake SNOTEL site there is much more pronounced precipitation seasonality, featuring a strong spring maximum, a weaker maximum in late fall/early winter, and a strong summer minimum. Altitudinal temperature gradient remains fairly constant year-round—slightly higher in the October-through-April snow-accumulation season (~6.5 °C/km) than in the May-through-September melt season (~5.9 °C/km)—(gradients computed from PRISM [Parameter-elevation Regressions on Independent Slopes Model—http://www.prism.oregonstate.edu/] monthly climate grids).

3. Previous work

3.1. Pleistocene glaciation

Atwood (1937) provided the first detailed description of Pleistocene glaciation in the northern Medicine Bow Mountains, mapping the icefield and describing paleoglaciers and their deposits in five major plateau/valley glacier complexes in the range. Much of this work focused on the southeastern quadrant of the range—the drainages of Libby and French Creeks—which is also the focus of this study. Atwood mapped and described deposits from two glaciations, which were termed the Wisconsin and pre-Wisconsin. Subsequent work by Ray (1940) and McCallum (1962) refined the chronology, and McCallum tentatively correlated the two glaciations originally identified by Atwood (1937) the Bull Lake (penultimate) and Pinedale (final) Pleistocene glaciations of the Wind River Range (Blackwelder, 1915), stratigraphic nomenclature that has been used since that time. Oviatt (1977) undertook detailed mapping and relative dating of deposits in the uppermost portion of the French Creek drainage, which he considered to be of combined glacial and rockfall origin ("till-protalus"), some of Holocene age.

Mears (2001) produced a series of somewhat generalized maps including a map of the extents of Pinedale, Bull Lake, and "pre-Bull Lake" glacial deposits across the range and maps of Bull Lake and multiple Pinedale deposits ("P1" and "P2") in the terminal area of the Libby Creek glacier, as well as of multiple younger Pinedale deposits ("P3" to "P5") in the upper portions of both Libby and French Creek drainages. The maximum extent of the Bull Lake and Pinedale glacial deposits in the range as mapped by Mears (2001) is shown in Fig. 2. In the vicinity of Centennial, Wittke et al. (2012) and Sutherland et al. (2013) remapped glacial deposits near the LLGM terminus of the Libby Creek glacier, based primarily on Mears' (2001) earlier mapping.

To date no numerical ages have been obtained for LLGM or older deposits in either the French or Libby Creek drainages, or elsewhere in the range. Basal radiocarbon ages from lake cores extracted for pollen analysis, taken within the LLGM ice margins (Mensing et al., 2011; Brunelle et al., 2013; Minckley, 2014), have provided some limiting ages for the last glacial maximum and subsequent deglaciation in the range, as is discussed in section 6.1.1 below.

Recently, Marcott et al. (2019) produced the first numerical ages for glacial deposits in the northern Medicine Bow Mountains. They obtained seventeen cosmogenic ^{10}Be exposure ages for the post-LLGM deposits at the base of the steep crest of the Snowy Range in the French Creek drainage, deposits previously mapped by Oviatt (1977), that Marcott et al. (2019) interpreted as three nested moraines. Marcott et al. (2019) reported mean exposure ages of 10.5 ± 0.3 (n = 4), 11.5 ± 0.5 (n = 6), and 14.5 ± 0.3 (n = 5) for the deposits, consistent with their relative positions in the drainage. In section 6 below we discuss these ages and their relationship to sixteen new surface-exposure ages on glacially transported boulders and glacially polished bedrock outcrops in the Libby Creek drainage that provide the first constraints on the timing of the last glacial maximum in the range.

3.2. Late Pleistocene paleoclimate

Relatively little is known about paleoclimate in the northern Medicine Bow Mountains during the LLGM and subsequent deglaciation. The previous studies of the glacial record discussed above did not focus on analysis of paleoclimate. Other proxy studies have, however, yielded qualitative information on paleoclimate in the range, notably for the deglaciation period and the Holocene. Paleoecological analysis of cores retrieved from several lakes in the range (Mensing et al., 2011; Minckley et al., 2012; Brunelle et al., 2013; Carter et al., 2013; Minckley, 2014) has indicated that following deglaciation, tundra vegetation prevailed and temperatures remained cooler than today from the earliest core ages of ~18–17 ka until ~12 ka when temperatures increased significantly, and that by about 9 ka temperatures were somewhat higher than today. Vegetation and lake levels at lower-altitude sites at Long Lake and Little Windy Hill Pond (Fig. 2 – Minckley et al., 2012; Carter et al., 2013; Shuman and Serravezza, 2017) suggest relatively dry conditions following deglaciation. At higher-altitude Little Brooklyn Lake (Fig. 2) it appears that moist conditions dominated during this interval, but this may reflect meltwater influx in an ice-proximal setting (Brunelle et al., 2013).

Studies in nearby areas have yielded somewhat divergent conclusions about climate during the LGM. Based on investigation of the distribution of fossil frost wedges in the Laramie Basin immediately to the east and north of the northern Medicine Bow Mountains (Fig. 1), and in other Wyoming basins, Mears (1981, 1987) concluded that mean-annual basin air temperatures during cold periods of the Pleistocene were at least 14 °C colder than today and that arid conditions prevailed in the basins. Climate-model output also suggests relatively large temperature depression, with moisture conditions generally similar to, or slightly drier than, today in region of the northern Medicine Bow Mountains (Oster et al., 2015; Lora et al., 2017; Oster and Ibarra, 2019). In contrast to evidence of large late Pleistocene temperature depressions from fossil frost wedges and climate models, glacier modeling studies in the northern Colorado Front Range, approximately 160 km south-southeast of the Snowy Range indicate smaller late Pleistocene temperature depressions (Dühnforth and Anderson, 2011; Gall et al., 2013).

4. Methods

4.1. Surface-exposure ages

In this study ^{10}Be surface-exposure dating was undertaken with two aims: first, to understand the timing of the LLGM in the northern Medicine Bow Mountains; and second, to understand the timing and rates of deglaciation following the LLGM. Our sampling effort focused on LLGM moraine boulders and glacially scoured bedrock surfaces in the Libby Creek drainage in the accessible southeastern quadrant of the LLGM icefield complex. In the neighboring French Creek drainage, LLGM moraine boulders proved unsuitable for exposure dating because of their highly weathered appearance, possibly due to fire-related fracturing. In light of the recently published exposure ages of Marcott et al. (2019) we also did not sample in the upper portions of the French Creek drainage.

4.1.1. Strategy and sampling

Our basic strategy was to collect and analyze at least six samples from moraine complexes and, when sampling polished-bedrock outcrops, to collect and analyze samples taken in close proximity to one another where possible. Due to a paucity of clear moraines in upper portions of the Libby Creek drainage, we sampled moraine boulders from only the LLGM terminal moraine complex (a total of six samples analyzed). Upvalley we collected and analyzed nine glacially polished-bedrock samples and one perched-erratic boulder sample, from outcrops representing times when the glacier had retreated by 35–40% to ~95% of its LLGM length.

All samples were collected using a hammer and chisel. In nearly all cases, samples were taken from portions of boulder or bedrock surfaces that showed clear evidence of glacial polish. Sample thicknesses ranged from 0.5 to 2.5 cm.

Moraine boulder samples were collected from upper surfaces of boulders firmly rooted in low-slope sections of moraine crests, generally with less than 10° surface slopes. Where possible samples were taken from a meter or more above the surrounding moraine surface, although a majority of the analyzed samples were taken from less than 1 m above the surface, one from less than 55 cm above the surface. A single 0.9 m-high perched boulder, sitting on a glacially polished surface upvalley of the terminal moraine complex was also sampled. Polished outcrop samples were taken from promontories that generally stood at least 1 m above surrounding areas of bedrock and/or soil. Samples were taken from low-slope (typically about 10°) portions of these outcrops.

4.1.2. Sample processing

Samples collected for cosmogenic ^{10}Be exposure dating were prepared at SUNY Geneseo for in-situ cosmogenic ^{10}Be measurement following methods in Laabs et al. (2013). Samples were crushed, milled, and sieved to a target grain size of 250–500 μm. Quartz grains were isolated using a rare-earth hand magnet, Franz magnetic separator, density separation, and dilute-acid treatment. The quartz-purification process was accomplished by repeated etching in dilute hydrofluoric and nitric acids (Kohl and Nishiizumi, 1992). Prior to dissolution in concentrated hydrofluoric acid, the purified quartz fraction of each sample was spiked with a commercially made ^{9}Be carrier solution. Procedural blanks were prepared using carrier mass (225–250 μg) equal to that added to samples. The beryllium fraction of each sample was chemically isolated and loaded into targets for ^{10}Be/^{9}Be measurement by accelerator mass spectrometry (AMS) at the Purdue University Rare Isotope Measurement Laboratory (Sharma et al., 2000;Muzikar et al., 2003). All ^{10}Be/^{9}Be values were corrected for measured procedural blank ratios of 5.66×10^{-15} to 5.86×10^{-15} and normalized to the AMS beryllium standard 07KNSTD (Nishiizumi et al., 2007).

4.1.3. Production rate and scaling

Exposure ages were calculated using the Balco et al. (2008) online exposure-age calculator, version 3.0 (http://hess.ess.washington.edu/math/). This calculator and version were selected because they implement the Lifton-Sato-Dunai nuclide dependent (LSDn; Lifton et al., 2014) scaling model and production rates based on user-defined calibration data from independently dated locations. Production rates were computed using *in situ* ^{10}Be data from the independently dated surface at the Promontory Point production-rate calibration site reported by Lifton et al. (2015), which features well-preserved and continuously exposed surfaces following the Bonneville Flood at 18,300 ± 300 cal Yr BP. This calibration site was selected because of its proximity in space and time to the study area, an approach that follows that of other recent reports of Pleistocene moraine chronologies in the Rocky Mountains (Licciardi and Pierce, 2018; Schweinsberg et al., 2020; Laabs et al., 2020). To ensure comparability, ages from Marcott et al. (2019) were recalculated using the same calibration site and at the same time (April 19, 2022) as the ages reported in this study, using the same production-rate and scaling schemes. Individual recalculated ages differed by no more than seven years from those originally reported by Marcott et al. (2019). Because nearly all of the sample surfaces came from either directly beneath or adjacent to areas of glacial polish, it appears that any post-glacial weathering of sample surfaces was extremely limited. Consequently we have made no weathering-related correction of exposure ages. We have also made no snow-shielding corrections. Both the height of boulder samples above the surrounding moraine and the sampling of bedrock promontories, primarily in windswept above-treeline sites, likely minimized snow cover at the sample sites. Nonetheless, the potential for snow shielding does introduce the possibility that reported ages are slight underestimates.

4.1.4. Reporting of individual and group ^{10}Be ages and uncertainties

We report individual ^{10}Be exposure ages with a 1σ analytical uncertainty ("internal uncertainty"). In instances where two or more ages were obtained from a single feature (a moraine or reconstructed ice margin) we report a group age as the mean of all sample ages with an uncertainty of ± one standard deviation of those ages (e.g. Laabs et al., 2020). We calculate a reduced χ^2 (i.e., the mean-squared-weighted-deviation) statistic for group age as a test of whether within-group age differences may be explained as a result of analytical uncertainty, or whether they indicate inter-sample age variability larger than can be explained by analytical uncertainty and thus suggest that the assumption that the samples are all of the same age is suspect (Barrows et al., 2002; Balco and Schaefer, 2006; Balco, 2011). Consideration of the reduced χ^2 value also allows us to assess whether the standard deviation is an appropriate measure of group-age uncertainty.

For comparison of ^{10}Be ages within the current study area and with the ^{10}Be ages of Marcott et al. (2019) from the adjacent French Creek drainage recalculated using the same production rate and scaling, it is appropriate to use uncertainties that incorporate analytical uncertainty but not production-rate uncertainty. However, for comparison to ages obtained using other chronometric methods or to ^{10}Be ages from more distant localities, production-rate uncertainties must be considered as well. Consequently in the latter situations we report individual ages with "external" uncertainty, and calculate group age uncertainties by summing in quadrature the standard deviation and the ±3.78% production-rate uncertainty, a value which we derived indirectly from ages yielded by the Balco et al. (2008) online exposure age calculator, version 3.0 (http://hess.ess.washington.edu/math/).

4.2. Glacier modeling

Glacier modeling was aimed first at establishing climate conditions that could have sustained the Libby and French Creek sectors of the Northern Medicine Bow Icefield Complex at their last glacial maximum extents. Because glacier mass balance is strongly controlled by both ablation-season temperature and accumulation-season precipitation, our modeling was aimed at establishing a suite of possible changes of

temperature and precipitation from modern conditions that would have sufficed to sustain the LLGM glaciers in mass-balance equilibrium. Our second goal in glacier modeling was to establish the magnitudes and timing of climate change that forced deglaciation of the valleys, making use of the deglaciation chronology established through surface-exposure dating.

The Plummer and Phillips (2003) 2-dimensional glacier model we used in this study is a coupled energy/mass-balance and flow model. The energy/mass-balance component calculates an annual net balance grid across the model domain, from inputs of digitized topography, modern climate, a set of instructions of how to alter model climate from the modern, and solar-insolation values adjusted for orbital geometry at the time period being modeled. Other model inputs include estimated snow and ice albedos, emissivity, and bulk-transfer coefficients. The model considers snow redistribution by avalanching, but not by wind.

The ice-flow component is a transient model that computes the changing glacier extent and thickness in response to the input climate, utilizing gridded output from the energy/mass-balance component as a distributed source term and employing a finite-difference solution to linearized equations for ice flow by internal deformation and basal sliding. Ice-flow velocity is determined at each grid node by Eq. (1),

$$u = u_d + u_s = \frac{2A}{n+2}\tau^n H + B\tau^m \quad \text{(Eq. 1)}$$

where u is total velocity, u_d and u_s are velocities due to internal deformation and basal sliding respectively, A and B are flow- and sliding-law coefficients respectively, n and m are flow- and sliding-law exponents, taken as 3 and 2 respectively, τ is the driving stress, and H is the ice thickness. Flow modeling is based on a shallow-ice approximation approach (Hutter, 1983) which relates driving stress to overlying ice thickness and surface slope.

Magnitudes of temperature and precipitation changes from present were varied to find combinations of the two which would result in a glacier in mass-balance equilibrium at the past extents that we were attempting to model. For each possible climate input, the two components of the model were run iteratively to account for changes in elevation-dependent climate parameters (temperature, precipitation, wind) and in topographic shading that would affect glacier-surface conditions as the glacier thickened or thinned. Details on the calculations used in both components of the model are given in Plummer and Phillips (2003) and in a subsequent series of papers which have introduced modifications (Laabs et al., 2006; Refsnider et al., 2008; Leonard et al., 2014, 2017b; Quirk et al., 2018, 2020). Our modeling used the methods outlined by Leonard et al. (2017b) where those differed from the methods of earlier papers.

4.2.1. Model scales

Glacier modeling was conducted at two different scales for computational efficiency. For modeling the LLGM glaciers and the initial phase of deglaciation, during which the icefield complex was still fairly extensive, modeling was conducted at 150 m resolution. For the final phases of deglaciation, when the complex was considerably smaller, modeling was done at 50 m resolution.

4.2.2. Model input

Ground-surface topography used in the glacier modeling was derived from USGS 10 m digital elevation models (https://www.usgs.gov/core-science-systems/ngp/tnm-delivery). Monthly temperatures and precipitation values were derived from 30-arc sec PRISM (Parameter-elevation Regressions on Independent Slopes Model – http://www.prism.oregonstate.edu/) grids of 1971–2000 C E monthly climate means, clipped to an area of 364 km^2 encompassing the Libby and French Creek drainages and the high plateau area to their south and east where our preliminary modeling indicated glacier extent may have been somewhat greater than previously mapped by Atwood (1937) and Mears (2001). For each individual pixel in the glacier-model domain monthly mean values of temperature and precipitation were determined from linear climate vs. elevation relationships for the clipped grids. Sources of other modern climate data are listed in Table 1, and other input parameters utilized in the energy/mass-balance modeling in Table 2.

Past studies have used a range of flow and sliding parameters in the flow component of the model (see Laabs et al., 2006; Leonard et al., 2017b, 2023 for fuller discussions). In this study we used the "soft-ice" parameters that Leonard et al. (2017b) found provided the best fit to southern Colorado paleoglaciers. These and other parameters used in flow modeling are listed in Table 2.

Sensitivity of model results to the inputs to both the energy/mass balance and the flow components is discussed in section 4.2.4 below.

4.2.3. Model validation

The optimal way to test the skill of the model and the appropriateness of the input modern climate data set and physical parameters (albedo, emissivity, wind-speed gradient, bulk-transfer coefficient, ice flow and sliding parameters, etc.) is to use the model as a predictor of the extent and thickness of modern glaciers within the model domain. Unfortunately, with modern glaciers absent from the northern Medicine Bow Mountains, this approach to validation could not be directly carried out. Instead, we followed approaches taken in other studies in areas without modern glaciers (e.g. Leonard et al., 2014, 2017b, 2023; Quirk et al., 2020), using two complementary approaches. First, we observed that some small snowfields in favored locations along the southeast side of the Snowy Range survive through most melt seasons, and these snowfields provided an opportunity for comparison to model results. Second, snow survey records are available for several sites within the model domain and the seasonal evolution of the snowpack at those sites could be compared to model simulation of snowpack evolution. Each of these approaches, however, has potential shortcomings. The mass balance of the small snowfields may be much more strongly influenced by localized factors such as wind drift of snow, avalanching and topographic shading than were the much larger Pleistocene glaciers we are attempting to model. While topographic shading and avalanche redistribution terms are included in the modeling, they are difficult to incorporate at the scale of very small snowfields, and wind drift of snow is not incorporated in the model. Snow survey sites, by contrast, are generally located in areas without significant topographic shading, wind drift or avalanche accumulation. However, since snow-survey data are available only for the time that snow remains on the ground, comparison of model simulations to them allows for assessment of the accumulation component of the energy/mass-balance model but only a limited assessment of the ablation component.

We located five sets of high-resolution aerial photographs taken during late August or September, over the interval of 1980–2014 C E. In Fig. 3 we compare average end-of-season snow cover with the area of snow accumulation predicted by the model based on "modern" climate input spanning the interval 1971–2000 C E. The model predicts only a few areas of accumulation (red pixels in Fig. 3), much smaller than the observed snowfields (blue areas in Fig. 3). To approximate the area of observed snowfields, model temperatures needed to be reduced by nearly 1.3 °C from modern (green pixels in Fig. 3). We suggest that the absence of a wind-drift term in the model results in lower-than-actual snow accumulation and explains our inability to simulate the small modern snow fields with modern climate input. Previous workers have indicated that the small snowfields are sustained primarily by wind drift of snow from the broad, low-relief high-altitude crest of the Snowy Range upwind to the north and west (Sommerfeld, 1994; Mensing et al., 2011). Mass balance studies on very small glaciers in similar topographic and climatic settings in the Colorado Front Range (Outcalt and MacPhail, 1965; Hoffman et al., 2007) indicate that wind drift is a primary source of accumulation. If the model's inability to reproduce these small snowfields is dominantly due to lack of a wind transport equations, then the 1.3 °C discrepancy is a very conservative indicator of the

Table 1
Modern climate data used in glacier modeling.

CLIMATE PARAMETER	DATA SOURCE	SITE	LATITUDE LONGITUDE	ALTITUDE (m)	DATES OF RECORD (CE)
Monthly mean temperature vs. altitude	PRISM 30-arc sec	Southeast quadrant of range	41° 12.3′ to 41° 24.3′ N 106° 6.7′ to 106° 27.0′ W	2452–3549	1971–2000
Monthly mean precipitation vs. altitude	PRISM 30-arc sec	Southeast quadrant of range	41° 12.3′ to 41° 24.3′ N 106° 6.7′ to 106° 27.0′ W	2452–3549	1971–2000
Monthly standard deviation of daily mean temperature, monthly mean percent of days with measurable precipitation[a]	SNOTEL (Snowpack Telemetry)	Brooklyn Lake	41° 21.5′ N 106° 13.9′ W	~3120	1989–2007
Monthly mean relative humidity, mean monthly wind speed	Glacier Lakes Ecosystems Experiments Site meteorological tower	West Glacier Lake	41° 22.5′ N 106° 15.5′ W	~3280	1991–2005

[a] Used as approximation of monthly mean cloud cover.

Table 2
Parameters used in glacier modeling.

MASS/ENERGY-BALANCE MODEL PARAMETERS	
Snow albedo	0.8
Ice albedo	0.4
Snow/ice emissivity	0.99
Basin emissivity	0.94
Wind k[a]	0.001msec^{-1}
Ground heat flux	0.1 Wm^{-2}
Bulk-transfer coefficient (snow)	0.0015
Bulk-transfer coefficient (ice)	0.00195
FLOW MODEL PARAMETERS	
Deformation-law coefficient (A)	2.5×10^{-7}yr^{-1}kPa^{-3}
Deformation-law exponent (n)	3
Sliding-law coefficient (B)	3.75×10^{-3}myr^{-1}kPa^{-2}
Sliding-law exponent (m)	2

[a] Change in wind speed per meter of altitude.

uncertainty of its application to Pleistocene paleoglaciers, for which wind transport would have been a relatively minor component of overall accumulation.

Fig. 4 compares modeled to observed mean end-of-month snow water equivalent (SWE) from three sites in the Libby Creek drainage, the only snow-survey sites located within the margins of the LLGM Libby or French Creek glaciers (see Fig. 1 for site locations). Modeled SWE values are based on PRISM monthly temperature and precipitation means from 1971 to 2000 C E and other model inputs detailed in Tables 1 and 2. SWE values for the Brooklyn Lake SNOTEL site at ~3120 m (Fig. 4a) are mean values from 1981 to 2000 C E (data from 1982 C E are missing), those from the snow courses at Hairpin Turn at ~2880 m (Fig. 4b) and Libby Lodge at ~2670 m (Fig. 4c) are mean values for 1971–2000 C E. The Brooklyn Lake SNOTEL records span the entire year, whereas at the two snow-course sites SWE data are available only for the peak months of snow cover (end-of-month measurements January through April). Overall, the modeled snowpacks correspond well with the observed snowpacks. At Brooklyn Lake (Fig. 4a) modeled and measured snowpacks correspond extremely well, except that the initial modeled springtime reduction in snowpack is slightly slower than the observed reduction. At Hairpin Turn (Fig. 4b), modeled snow accumulation is slightly less than the observed during the early season, but the initial reduction of modeled snowpack takes place later than that of the observed snowpack. At Libby Lodge (Fig. 4c) early season modeled accumulation is again slightly less than observed, but in this case the observed snowpack persisted later in the spring than the modeled snowpack. It should be expected that fairly minor differences of the sort just discussed would occur between modeled and observed snowpack evolution, as snowpack modeling is based on regional climate characteristics, whereas site-specific snowpack records reflect both regional climate and local site characteristics.

The above discussion suggests that the model does a good job of simulating snowpack evolution from input climate in areas without significant topographic shading, avalanching, or wind drift of snow. The model has a more difficult time simulating small semi-permanent snowfields in areas where these processes are more important. We discuss the implications of this for a quantitative assessment of model uncertainty in the next section.

4.2.4. *Overall model uncertainty*

The validation tests discussed above provide insight into model uncertainty related to the ability of the model to simulate modern snowpack from modern climate input. Other uncertainties arise when the model is applied to paleoglaciers in an attempt to assess paleoclimate and in the coupling of the energy/mass-balance and ice-flow components of the model. In this section we characterize model uncertainty as the uncertainty in paleotemperature estimated for a given paleoprecipitation. Although we believe that uncertainty discussed above in modeling the small snowfields from modern climate input is likely a significant overestimation of the uncertainty when the model applied to the much larger Pleistocene glaciers, we take a conservative approach and assume a ±1.3 °C uncertainty in temperature estimates derived from the model when it is used to simulate glacier mass balance from input climate data. We treat this as an uncertainty, rather than a correctable error, because in other instances modeling of small, topographically favored snowfields results in an overestimation, rather than an underestimation, of snowfield extent. In the Colorado Sangre de Cristo Mountains, for example, Leonard et al. (2017b) found that in a setting where wind drift appears to be less of a factor (Refsnider et al., 2009) and accumulation to be more strongly influenced by avalanching, the model produced an overestimation of the area of small modern snowfields. This example, combined with the issue of modeling wind-drifted snow described above, attests to the difficulty of accurately modeling very localized processes of accumulation and ablation. It appears that application of the model to small snowfields in topographically favored locations may result in either underestimation or overestimation of snowfield extent.

Quirk et al. (2020) have recently run tests to assess the sensitivity of model paleotemperature output to additional climate inputs including albedo, cloudiness, wind speed, relative humidity and bulk-transfer coefficient, concluding that likely past ranges of these characteristics collectively result in an uncertainty in modeled paleotemperature of about ±1.0 °C. In previous work the current authors and their collaborators (Leonard et al., 2014, 2017b, 2023, unpublished data) have run analyses to test the sensitivity of model results to likely ranges of ice deformation and sliding parameters and to the effect of chronological uncertainties on the insolation parameters used in the modeling. Summing all these independent error sources in quadrature, including the ±1.3 °C discussed in the previous paragraph, results in an overall model uncertainty of ±1.7 °C. While there are other possible sources of uncertainty that we are not able to quantify, particularly potential past changes in altitudinal gradients and seasonality of temperature and precipitation, we feel that in view of the conservative approach we have

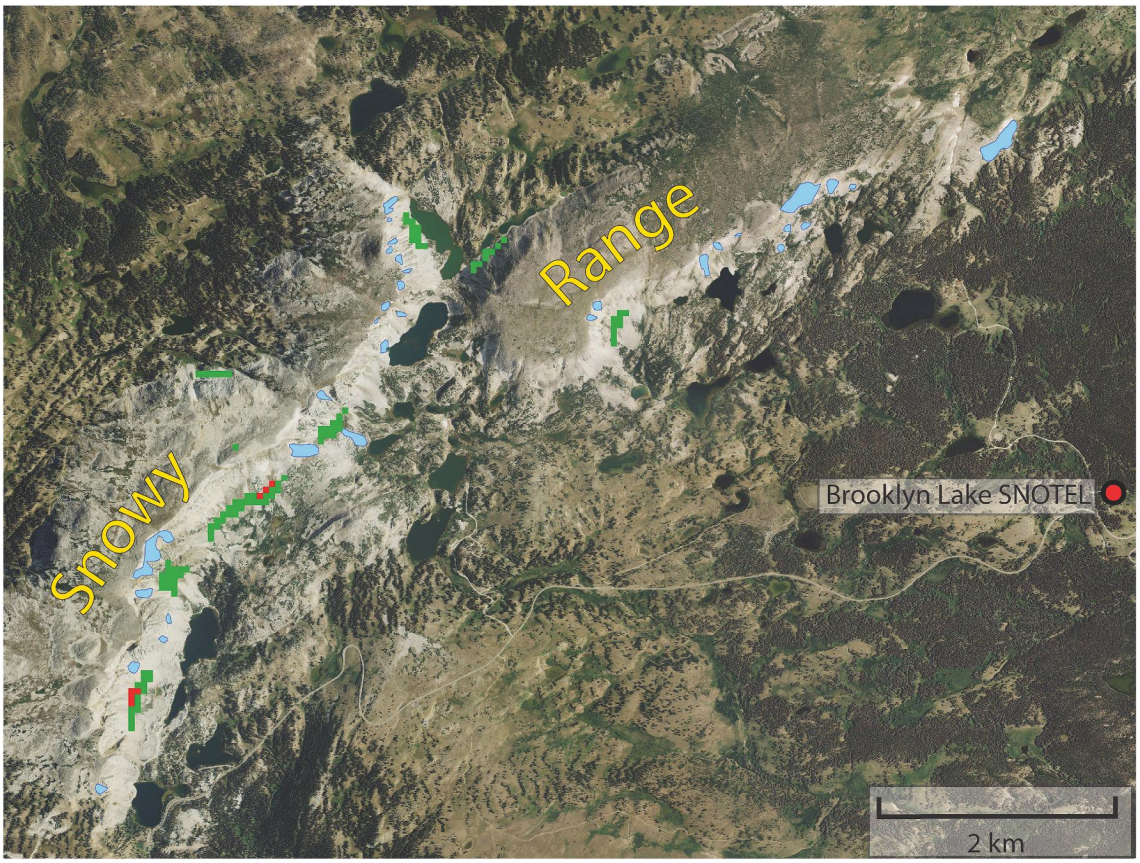

Fig. 3. Energy/mass balance model validation results I. Blue indicates approximate "average" location and extent of end-of-summer snowfields derived from five sets of late August or September aerial photos taken between 1980 and 2014 CE. Red squares are model 50 m pixels with end-of-season net accumulation based on 1971–2000 CE climate input with no change in temperature or precipitation. Green indicates model pixels with end-of-season net accumulation based on a 1.3 °C depression of temperature from 1971 to 2000 CE means with no other change from 1971 to 2000 CE conditions. Red circle indicates location of the Brooklyn Lake SNOTEL site utilized in additional validation study (Fig. 4a). (For interpretation of the references to colour in this figure legend, the reader is referred to the Web version of this article.)

taken to uncertainty in the ability of the model to simulate glacier mass balance from input climate data, this overall uncertainty value of ±1.7 °C is appropriate.

4.3. Climate-model comparisons

We compare our glacier-model simulation results from the northern Medicine Bow Mountains to global climate-model output drawn from the Paleoclimate Model Intercomparison Project Phase III (PMIP3 – https://pmip3.lsce.ipsl.fr [last accessed 2022-11-8]), the Transient Climate Evolution of the last 21 thousand years intercomplexity model simulation (TraCE 21ka—Lorenz et al., 2016), and the Osman et al. (2021) proxy-constrained reanalysis of global mean temperature evolution since the LGM (LGMR). While PMIP3 includes nine separate simulations of the LGM (21 ka) Earth, we compare our glacier-model output to the five PMIP3 simulations that Oster et al. (2015) identified as providing the best fits to LGM precipitation proxies across western North America. TraCE 21ka and the LGMR are transient models that span the last 22,000 and 24,000 years, respectively. The PMIP3 and TraCE 21ka model output includes both temperature and precipitation fields, whereas the LGMR includes only temperature fields. Because glacier mass balance is most strongly controlled by ablation season (summer) temperature and accumulation season (fall-through-spring) precipitation (Ohmura et al., 1992; Oerlemans, 2001) we compare our glacier-simulation results to both annual and seasonal climate-model output: namely, June–August temperatures, and October–April precipitation. For the PMIP3 and TraCE 21ka models, we have interpolated model output to the approximate position of the LLGM glacier equilibrium line of the Libby drainage glacier using bilinear interpolation methods (Oster and Ibarra, 2019). For the LGMR we have used the mean value of the two model tiles that encompass the Northern Medicine Bow Icefield Complex.

Direct comparisons are made more difficult by differences in scales of available model output, in modeling timestep, and in the different models' modern or preindustrial (PI) baseline time intervals to which paleotemperatures are compared. Further, topographic complexity is smoothed at the resolution (~1–3°) that climate models are run, not capturing high elevation peaks in topography. In our glacier modeling, paleoclimate is characterized as the difference between paleo-conditions and "modern" temperature and precipitation means for the interval 1971–2000 C E. In PMIP3 model output, LGM (21ka) conditions are compared to PI conditions (~1850 CE). Using the TraCE 21ka output, we compare paleo-conditions to a PI interval we define as 1750–1850 CE, whereas the LGMR is referenced relative to the last 2000 years (following Osman et al., 2021). For the transient climate-model simulations—TraCE 21ka and the LGMR—we define LGM conditions as those of the coldest 1000-year interval.

5. Results

5.1. Glacial chronology

Field and laboratory data for samples collected for cosmogenic ^{10}Be exposure dating are given in Tables 3 and 4 and S-1, and exposure ages

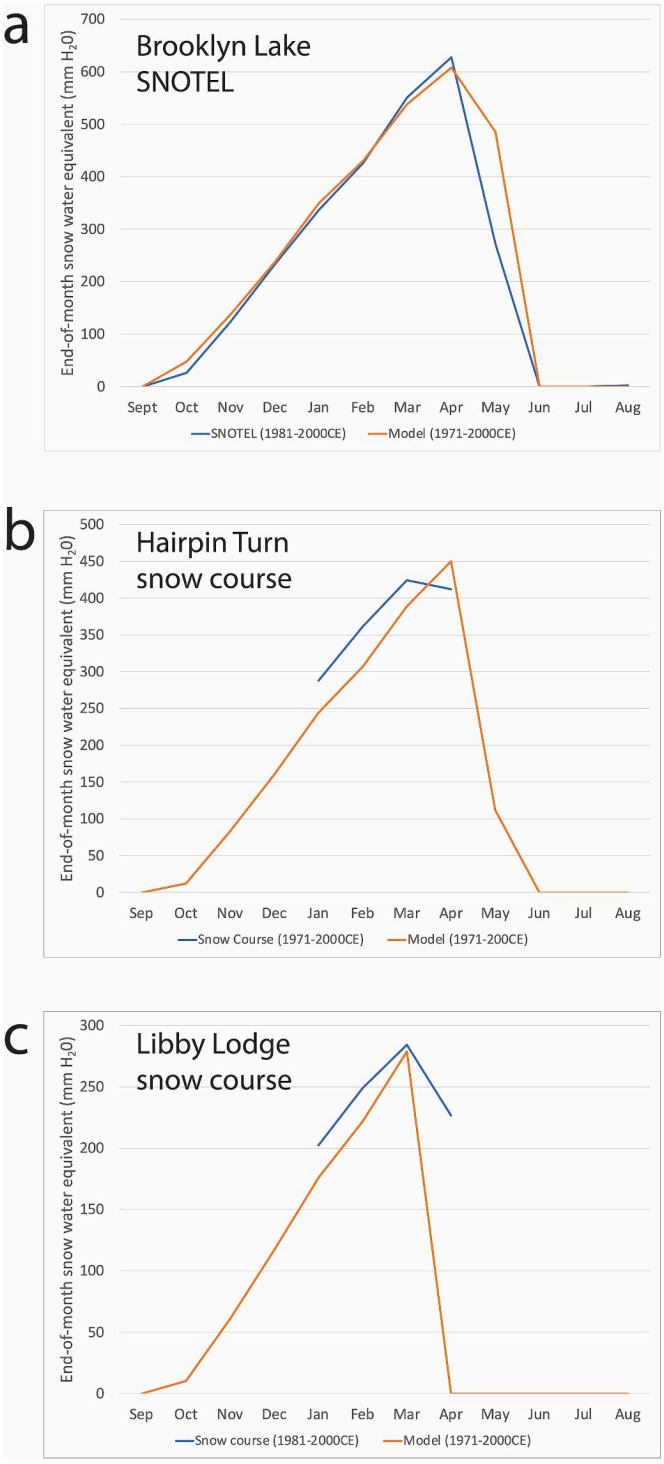

Fig. 4. Energy/mass balance model validation results II. Comparison of seasonal snowpack evolution predicted by model (brown curves) with snow-survey data (blue curves). (a) Brooklyn Lake SNOTEL mean end-of-month snowpack vs. model-predicted snowpack for the site; (b) Hairpin Turn snow course mean end-of-month snowpack vs. model-predicted snowpack for the site; (c) Libby Lodge snow course mean end-of-month snowpack vs. model-predicted snowpack for the site. Note that at Horseshoe Turn and Libby Lodge the snow-course data cover the same years as the model input climate. At Brooklyn Lake the SNOTEL data cover only the final ~2/3 of the model input period. (For interpretation of the references to colour in this figure legend, the reader is referred to the Web version of this article.)

are plotted in Figs. 5 and 6. Ages from Marcott et al. (2019) are also plotted in the figures.

5.1.1. *Exposure ages from the Libby Creek LLGM terminal moraine complex*

We report ^{10}Be exposure ages of six boulders atop moraines in the Libby Creek LLGM terminal complex (Fig. 5c and 6, Tables 3 and 4 and S-1), a complex that extends about a kilometer along the Libby Creek valley floor. In the most distal portion of the complex a discontinuous right-lateral ridge is the outermost feature (Fig. 5c). This ridge, which does not contain appropriate boulders for cosmogenic exposure dating and was not sampled, may represent the maximum extent of ice during the last glaciation or may have formed during an earlier advance. Five boulders were sampled from the broad outermost continuous moraine, inside the unsampled moraine fragment. Four of the boulders (SR10-03, SR10-09, SR11-03a, SR11-04) yielded ages ranging from 17.4 ± 0.5 ka to 23.7 ± 1.2 ka, with a mean of 20.7 ± 2.8 ka. The fifth sample (SR11-02) yielded an exposure age of 143.7 ± 2.6 ka. The single boulder (SR11-01) from the inner portion of the moraine complex yielded an age of 16.1 ± 0.5 ka.

5.1.2. *Libby Creek drainage polished-bedrock and perched-boulder ages*

We collected and analyzed ten samples, nine from polished-bedrock outcrops and one from a boulder perched on such a bedrock outcrop, taken from the middle and upper portions of the glaciated Libby Creek drainage (Figs. 5 and 6, Tables 3 and 4 and S-1). Broadly the samples fell into three groups, representing approximately 38%, 75%, and >90% reduction of Libby drainage glacier length from its LLGM extent.

Samples SR12-04 and SR10-08, a polished-bedrock sample and a polished boulder perched on the bedrock surface about 25 m away, both in a position that would have been exposed with ~38% reduction in length of the LLGM glacier (Fig. 5a and 6), yielded ages of 18.4 ± 0.9 ka and 17.7 ± 0.7 ka respectively (mean = 18.0 ± 0.4 ka). Upvalley, in a position that would have been exposed with ~75% reduction in glacier length, a single polished-bedrock sample (SR10-06) yielded an age of 14.7 ± 0.4 ka (Fig. 5b and 6).

Seven more polished-bedrock samples were analyzed from areas that would have been ice covered until >90% deglaciation of the drainage had occurred (Fig. 5b and 6). Those samples yielded ages ranging from 13.7 ± 0.3 ka to 14.6 ± 0.4 ka, with a mean of 14.2 ± 0.3 ka.

5.2. *Glacier-modeling results*

Using the Plummer and Phillips (2003) coupled energy/mass-balance and flow model, we reconstructed both the LLGM icefield complex in the northern Medicine Bow Mountains (Fig. 7), and various stages of deglaciation, linked to the exposure ages reported above. Because the upper portions of the range were occupied by generally contiguous icefields, we modeled the entire complex as a single domain, with a single climate input, recognizing that this approach ignores any differences in climate across the range—most likely cross-range difference in precipitation. We focused our attention on matching modeled ice extent to mapped ice extent in the Libby and French Creek drainages, from which our modern climate input to the model was derived. The magnitude of climate change from present conditions necessary to sustain the paleoglaciers was quite similar between these two valleys. By contrast, in other portions of the range, models that fit the Libby and French Creek glaciers either underestimated (typically in the west and north) or overestimated (in the northeast) the mapped extent of LLGM glaciers.

5.2.1. *LLGM conditions*

Fig. 7 illustrates model output with a 6.0 °C annual temperature depression (with temperature depressed uniformly each month) coupled with no change from modern precipitation amounts and seasonality, and no other changes from modern climate input, other than orbitally

Table 3
^{10}Be exposure ages of moraine boulders, erratic boulders, and glacially scoured bedrock.

Sample ID	Surface	Latitude (°N)	Longitude (°W)	Elevation (m)	^{10}Be exposure age (ka)	Internal uncertainty (kyr)	External uncertainty (kyr)
Terminal moraine complex (outer)							
SR10-03	Moraine boulder	41.3200	106.1515	2608	19.6	0.6	0.9
SR10-09	Moraine boulder	41.3164	106.1543	2616	23.7	1.2	1.5
SR11-02	Moraine boulder	41.3166	106.1536	2617	143.7	2.6	6.2
SR11-03 A	Moraine boulder	41.3162	106.1542	2613	17.4	0.5	0.8
SR11-04	Moraine boulder	41.3163	106.1559	2619	22.2	0.5	1.0
Terminal moraine complex (inner)							
SR11-01	Moraine boulder	41.3194	106.1592	2604	16.1	0.5	0.8
Mid-drainage paired samples							
SR10-08	Erratic boulder	41.3504	106.2107	3040	17.7	0.7	1.0
SR12-04	Bedrock	41.3502	106.2110	3047	18.4	0.9	1.2
Upper drainage (distal site)							
SR10-06	Bedrock	41.3558	106.2748	3276	14.7	0.4	0.7
Upper drainage (proximal sites)							
SR12-01 A	Bedrock	41.3758	106.2607	3313	13.7	0.3	0.6
SR12-03	Bedrock	41.3626	106.2840	3336	14.0	0.5	0.7
SR13-01	Bedrock	41.3646	106.2989	3328	14.6	0.4	0.7
SR13-02	Bedrock	41.3645	106.2994	3322	14.1	0.7	0.8
SR13-03	Bedrock	41.3627	106.3040	3328	14.5	0.3	0.6
SR13-04	Bedrock	41.3627	106.3039	3324	14.4	0.4	0.7
SR13-05	Bedrock	41.3627	106.3036	3311	14.1	0.5	0.7

Note: Exposure ages reported here were computed with the Version 3.0 online calculator (Balco et al., 2008; http://hess.ess.washington.edu) using a calibrated production rate from Promontory Point, Utah (Lifton et al., 2015), and the "LSDn" scaling model (Borchers et al., 2016). Internal uncertainty reflects ^{10}Be measurement error, external uncertainty includes both measurement and production-rate error. Sample data and additional age calculations are included in the data supplement.

corrected insolation to 21 ka, our best estimate of the timing of the LLGM based on the mean ^{10}Be exposure age of the terminal moraine. The modeled icefield has an area of 591 km^2, a maximum thickness of 373 m and a mean thickness of 134 m. Modeled glacier equilibrium line altitude (ELA) was approximately 3090 m. This model slightly overestimates the mapped LLGM extent of the Libby Creek glacier and slightly underestimates that of the French Creek glacier. Our best-fit estimate of the annual temperature depression necessary to sustain the LLGM glacier in the Libby Creek drainage absent any change from modern precipitation is ~5.9 °C, in French Creek drainage, ~6.1 °C.

Of course, multiple climatic characteristics in addition to mean temperatures may have changed between the LLGM and the present, including total precipitation, altitudinal gradients of temperature and precipitation, seasonality, windiness, and cloudiness. As the primary controls on mid-latitude glacier mass balance are accumulation-season precipitation and ablation-season temperature (Ohmura et al., 1992; Oerlemans, 2001), we focus on combinations of changes in mean temperature and precipitation that could result in a glaciers of mapped extent. We ran the model to solve for temperature depression necessary to produce a glacier in mass-balance equilibrium at LLGM extent in each valley with precipitation of 50%, 100%, 150%, and 200% of modern. These results are plotted in Fig. 8, with a 2nd order polynomial best-fit lines to the four model results for each valley also plotted. Over this range of possible LGM precipitation, necessary temperature depression in the Libby Creek drainage ranges from 3.1 °C at twice modern precipitation to 7.9 °C at half modern precipitation, in the French Creek drainage from 3.2 °C at twice modern precipitation to 8.1 °C at half modern precipitation.

5.2.2. Deglaciation simulations

We also modeled changes from modern temperature that could have sustained the Libby Creek glacier in mass-balance equilibrium at the extents that would just uncover the three sets of upvalley surface-exposure-dating sites with ages of 18.0 ± 0.8, 14.7 ± 0.4, and 14.2 ± 0.3 ka (for reasons discussed in section 6.1 below, the uncertainty on the first of these ages is considered to be 0.8 kyr, rather than 0.4 kyr). In these simulations we did not change overall precipitation or climate variables other than year-round temperature from modern values. A temperature depression of ~5.0 °C would be necessary to sustain the glacier at its recessional length of ~62% maximum at 18.0 ± 0.8 (Fig. 9a), assuming no change from modern precipitation, a 4.4–4.5 °C temperature depression at 14.7 ± 0.4 ka at about 25% of its maximum length (Fig. 9b), and a ~4.2 °C temperature depression at its recessional length of only 5–10% maximum at 14.2 ± 0.3 ka. (Fig. 9c). Over the same time interval, the entire icefield complex would have diminished from about 35% to only about 4% of its LLGM area (Table 5). At 14.2 ± 0.3 ka the modeled ELA had risen to about 3360 m. As discussed in section 6.2 below, interpretation of these model results depends on an understanding of the response time of the icefield complex and whether it is appropriate to assume that its extent was in approximate equilibrium with climate over each of the time intervals considered.

6. Discussion

6.1. – LGM and deglaciation chronology

Moraine-boulder exposure ages are generally interpreted to indicate the timing of initial recession of the active ice margin from the position of the moraine (Briner et al., 2005; Balco, 2011; Laabs et al., 2020). Exposure ages on the Libby Creek LLGM terminal-moraine complex are somewhat scattered and do not definitively resolve the timing of initial recession. Four of the five boulders sampled on the outer moraines of the complex yielded ages during or closely following the global LGM interval (26.5–19 ka—Clark et al., 2009). The fifth sample yielded an anomalously old age (SR-11-02—143.7 ± 2.6 ka) likely reflecting ^{10}Be inheritance, possibly as a reworked boulder from the penultimate glacial maximum. The other four ages suggest a range for possible timing of initial recession (17.4 ± 0.5 ka to 23.7 ± 1.2 ka—mean 20.7 ± 2.8 ka).

The reduced χ^2 value (~21.0) for the four ages on the outer terminal complex is far greater than unity (Table 4) indicating that the range of ages exceeds that expected based on the analytical uncertainty alone. This suggests that the samples either do not represent a single event or that there are sample-to-sample differences in exposure history. While the youngest-aged sample is responsible for much of the elevated reduced χ^2 value, the χ^2 value for the remaining three ages (9.4) is still far greater than could be explained by analytical uncertainty alone. There is difference of opinion concerning how to interpret such a range of ages on a moraine. While some workers argue that the oldest age is most representative (Applegate et al., 2010; Heyman et al., 2016), others consider the mean age after excluding clear outliers to be more

Table 4
Interpretation of ice-marginal ages and uncertainties based on multiple ages from individual features[a].

Location Sample IDs	Mean exposure age (ka)	1σ standard deviation (kyr)	1σ uncertainty including production rate uncertainty (kyr)	Reduced χ^2	Interpretation
Terminal moraine complex (outer)					
SR10-3, SR10-9; SR11-3a; SR 11-4[a]	20.7	2.8	2.9	21.04	Reduced χ^2 »1 indicates overdispersed distribution of sample ages, suggesting that samples may represent multiple events
Mid-drainage paired samples					
SR10-8; SR 12-4	18.0	0.5[b]	0.8[b]	0.34	Reduced χ^2 »1 indicates overdispersed distribution of sample ages, suggesting that samples may represent multiple events
Upper drainage (proximal sites)					
SR12-1A; SR12-3; SR13-1; SR13-2; SR13-3; SR13-4; SR13-5	14.2	0.3	0.6	0.81	Reduced $\chi^2 \sim 1$ indicates normal distribution of sample ages. Samples likely represent a single age event, with the standard deviation an appropriate measure of age uncertainty.

Calculations were made based on unrounded ages (reported in Tables S–1) and age results were then rounded to the nearest 0.1 ka or kyr.
[a] Sample SR11-02 is considered an outlier and in not included in this dataset.
[b] Due to the very low χ^2 statistic, these values are considered underestimates of group uncertainty. As discussed in section 6.1 we use the two-sample means of the internal and external uncertainty values, 0.8 and 1.1 kyr respectively, as the group uncertainty values.

appropriate. The latter approach has been followed in the nearby Colorado Rocky Mountains (Briner, 2009; Leonard et al., 2017a, 2017b; Laabs et al., 2020; Schweinsberg et al., 2020), as well as by Marcott et al. (2019) in the upper French Creek drainage, is the approach taken here. This suggests that recession from the outer portion of the LLGM terminal moraine complex began around 20.7 ± 2.8 ka, although we recognize that this is not a tight constraint on the timing of initial recession, and that the samples may in fact represent more than one LLGM glacial event.

It is difficult to constrain when final abandonment of the entire terminal moraine complex at Libby Creek occurred. The single available age for an inner moraine in the complex (SR11-01—16.1 ± 0.5 ka), viewed in conjunction with the youngest age from the outer moraines (SR11-03A—17.4 ± 0.5 ka), suggest that the glacier may have remained at, or close to, its LLGM extent until 17–16 ka. While this is consistent with behavior documented in several other areas of the Rocky Mountains (e.g. Leonard et al., 2017a; Laabs et al., 2020; Tulenko et al., 2020), two overlapping ages further upvalley suggest that significant recession had occurred before this time.

The paired exposures ages from polished bedrock and a polished boulder perched on that bedrock outcrop, at face value, suggest that the Libby Creek glacier had lost ~38% of its length by about 18 ka, apparently inconsistent with the youngest moraine-boulder ages just discussed (Fig. 6). Given the very low reduced χ^2 value and very small sample size that this site (Table 4) we conclude that the standard deviation of the two sample ages (1σ = ± 0.4 kyr) probably underestimates group-age uncertainty, and we feel that the mean of the internal uncertainties of the two sample ages (±0.8 kyr) is a better indication of group-age uncertainty. Even with the larger uncertainty, the paired upvalley ages, which imply significant deglaciation by about 18.0 ± 0.8 ka, seem inconsistent with the two younger ages in the terminal moraine complex. It is possible that the youngest moraine boulders yielded ages that are too young – possibly as a result of post-depositional disruptions of continuous exposure. Alternatively, it is possible that the two upvalley ages are too old. In this case, both upvalley ages might reflect a degree of inheritance, because of limited erosion of the bedrock outcrop and because the erratic was transported to this locality with a small inherited inventory of ^{10}Be. However, given the consistency of the two ages and the two entirely separate processes which would have caused inheritance problems with the two samples, this seems a less likely explanation. Consequently, our preferred interpretation is that significant ice recession had occurred by about 18 ka, that ice did not subsequently readvance to the terminal complex, and that the two young ages on boulders in the terminal complex likely reflect post-depositional shielding. It is possible, given the many individual moraine crests in the terminal complex and the relatively wide scatter of ages, and consequent high reduced χ^2 value, even on its outermost portions, that the complex was occupied multiple times between the LLGM and the final recession of ice from the vicinity of the complex, most likely by 18 ka.

An initial concern with exposure dating in the upper portion of the Libby Creek drainage was that on the extensive Libby Flats surface, particularly in areas where ice was not channeled down shallow valleys but was a drape over broad interfluves, nuclide inheritance might be a significant problem. In interfluve areas ice might have been thin and slow moving enough to limit erosion of the hard quartzite bedrock. Somewhat surprisingly, however, the ages were consistent site-to-site, whether a sample was from a scoured valley site or an interfluve site. Any inheritance affecting the ages, then, would have been of very similar magnitude between all sample sites, something we consider quite unlikely. Consequently, we interpret the polished-bedrock ages from the upper portion of the Libby drainage to be good indicators of the times at which the ice margin retreated across the sample sites. The farthest downvalley site (SR10-06), which would have been uncovered when ice retreated to about 75% of its LLGM length, yielded the oldest age (14.7 ± 0.4). The seven samples upvalley, which would have been exposed only after the ice margin had receded by 90% or more, all yielded younger ages. The reduced χ^2 value for those seven ages is 0.81 (Table 4) indicating that the scatter among them is approximately what would be expected due to analytical uncertainty, and thus that the samples may be treated as indicating the timing of a single deglaciation event occurring at 14.2 ± 0.3 ka. Consequently, we conclude that by shortly after 15 ka the ice margin had retreated to the point that along the main flowline the Libby Creek glacier was only about 25% of its LLGM length, and by ~14 ka the glacier margin had retreated to only 5–10% of its LLGM length.

In the French Creek drainage (immediately to the south of the Libby Creek drainage, Fig. 2) dating of small moraines at the base of the Snowy Range scarp by Marcott et al. (2019) indicated that the main valley was deglaciated by ~14.5 ka, at which time either a standstill or a small readvance of ice occurred (Fig. 6). Subsequent, even less extensive, readvances (or pauses during final deglaciation) occurred around 11.5 and 10.5 ka. Our model results, discussed in sections 5.2.2 above and 6.2 below, indicate that at the time the uppermost seven Libby drainage sites were being deglaciated (~14.2 ± 0.3 ka), ice would have been extremely limited in the area where Marcott et al. (2019) documented only very limited possible ice-marginal readvances (or standstills) after 14.5 ka (Fig. 9c).

6.1.1. Comparison of surface-exposure ages and basal-sediment radiocarbon ages

Our LLGM and deglaciation chronology is broadly consistent with basal-sediment ages that have been retrieved from several lakes in the range, although in some instances the basal ages are somewhat older

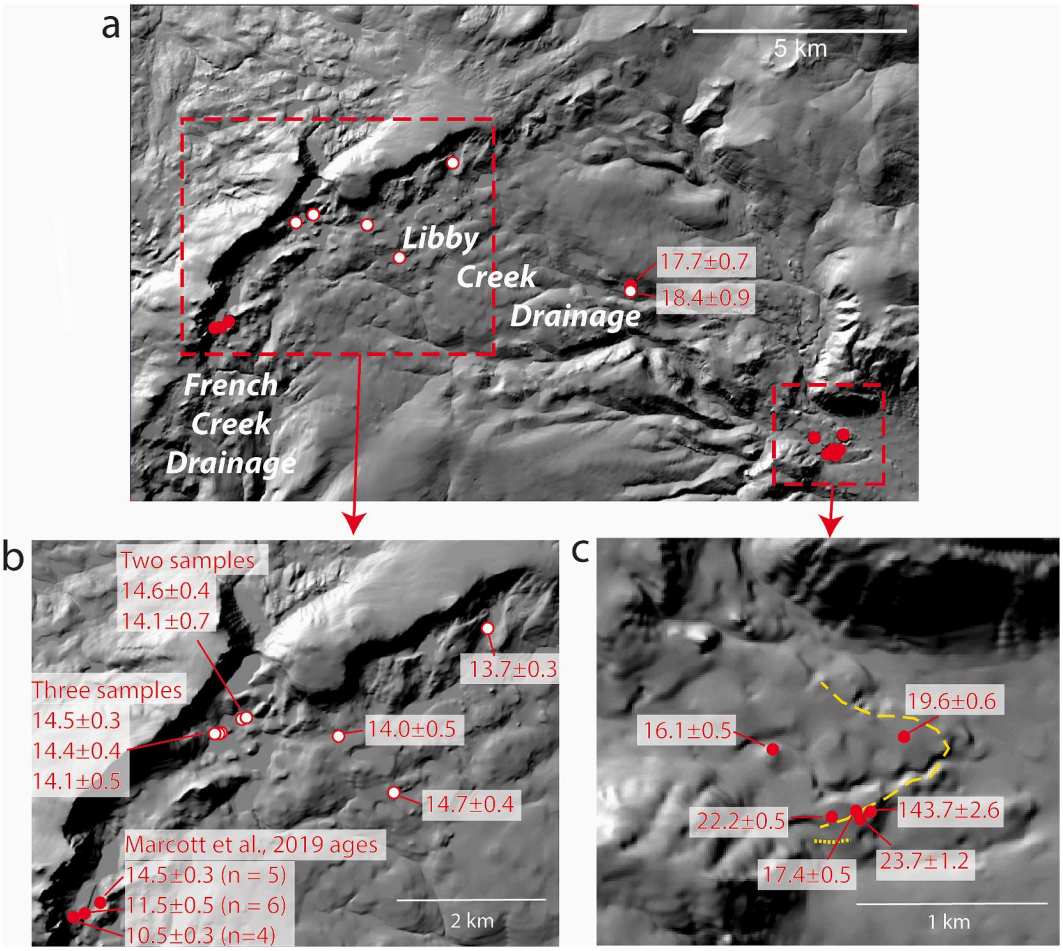

Fig. 5. Location of ^{10}Be exposure ages in Libby Creek drainage (this study) and French Creek drainage (Marcott et al., 2019). Individual ages in Libby Creek drainage are shown with 1σ internal uncertainty, mean ages from deposits in French Creek drainage are shown in frame b with 1σ standard deviation. (a) Location of all samples in both drainages. Closed circles indicate boulder samples, open circles are polished-bedrock samples. Ages are shown for paired bedrock and boulder samples in the middle portion of the Libby Creek drainage in this panel. All other sample ages are shown in the two enlarged panels. (b) Samples from the upper portion of the two drainages. Individual ages are shown for Libby Creek drainage polished-bedrock samples reported in this study. Unit mean ages are shown for French Creek drainage moraine-boulder samples previously reported in Marcott et al. (2019). (c) Individual sample ages of moraine boulders in the Libby Creek drainage LLGM terminal-moraine complex. Yellow dashed line is the approximate position of the outermost continuous moraine crest of the complex. Yellow dotted line indicates the approximate position of an undated discontinuous more-distal moraine fragment that may represent a maximum LLGM ice position or may have been deposited during an earlier advance. (For interpretation of the references to colour in this figure legend, the reader is referred to the Web version of this article.)

than associated exposure ages. Following Stuiver et al. (2021) we report the calibrated ranges of radiocarbon ages to the nearest ten years. In this comparison we report exposure-age uncertainties which reflect production-rate uncertainties as well as analytical uncertainty—"external" uncertainty for individual ages and standard deviation summed with production rate uncertainty for group ages (Table 4).

Long Lake, which is impounded by LLGM moraines on the northern flank of the range (Fig. 2), yielded a near-basal microfossil calibrated radiocarbon age of 11,980–12,390 cal yr BP (2σ range), leading to an extrapolated basal age of 12,540 cal yr BP (Carter et al., 2013). While this age is considerably younger than our exposure-age-based estimate of the timing of initial recession from the LLGM moraines in the Libby drainage (20.7 ± 2.9 ka), it is only a minimum age and past experience indicates that basal ages from lakes impounded by moraines may be significantly younger than the impounding moraines (Davis and Davis, 1980). Further upslope on the northern flank of the range a near-basal bulk-sediment age of 17,120–17,440 cal yr BP (2σ range) was obtained at Little Windy Hill Pond (Fig. 2; Minckley et al., 2012). The site is well within the LLGM ice margin and according to our modeling (section 5.2.2) was still covered by ice at 18.0 ± 0.8 ka, consistent with the basal-sediment age.

Within the Libby Creek drainage, basal ages from lake cores are available at three sites. At Little Brooklyn Lake (Fig. 2), which is well within the LLGM ice margins and which our modeling indicates was also still ice covered at about 18 ka (Fig. 9a), basal sediment yielded a bulk-sediment age of 26,600 ± 390 ^{14}C yr BP (calibrated to 30,050–31,280 cal yr BP—95% certainty range), and another age of 17,680–18,520 cal yr BP (2σ range) was obtained from bulk sediment approximately 40% of the distance above the base of the core (Brunelle et al., 2013). The basal age at Little Brooklyn is clearly inconsistent with the exposure ages. It could reflect a sediment package that predated, but survived, the last glacial maximum, or it could reflect problems with bulk-sediment dating in an area of carbonate bedrock (Houston and Karlstrom, 1992). At higher altitude in the Libby drainage on quartzite bedrock (Houston and Karlstrom, 1992), Mensing et al. (2011) reported a near-basal sediment age of 14,890–15,140 cal yr BP (2σ), from which they extrapolated a basal age of 15,330 cal yr BP, from East Glacier Lake (Fig. 2), an area which our modeling (section 5.2.2) suggests was deglaciated between about 14.7 ± 0.7 ka and 14.2 ± 0.6 ka (Fig. 9b + c). Minckley (2014) reported a somewhat older (16,460 cal yr BP) extrapolated basal age from nearby West Glacier Lake, also on quartzite bedrock (Houston and Karlstrom, 1992), but had little confidence in that

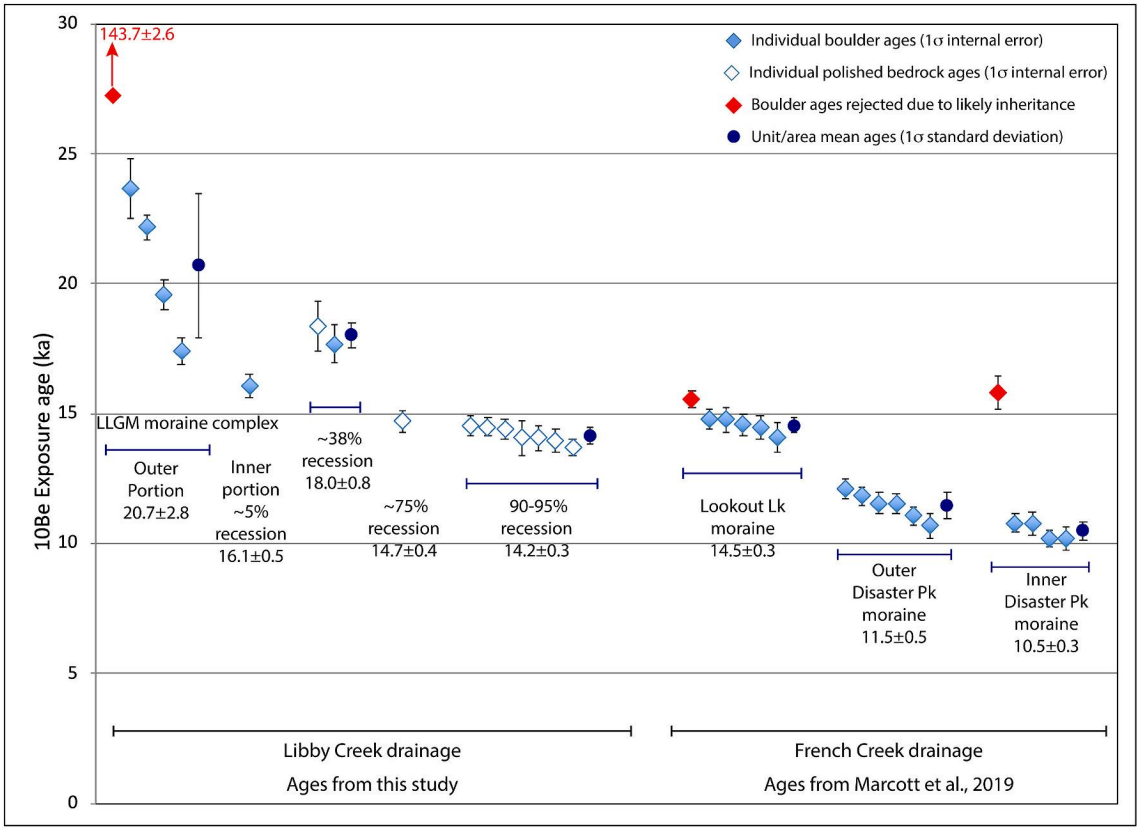

Fig. 6. Glacially transported boulder and polished-bedrock ^{10}Be exposure ages in Libby Creek drainage plotted at left by age and position in drainage. Moraine-boulder ages in the upper portion of French Creek drainage (Marcott et al., 2019) are plotted to right by age and moraine sequence, with progressively upvalley moraines plotted left-to-right. Numerical ages and uncertainties listed below the plotted samples are sample age and internal error for ages assigned based on a single sample or group mean and standard deviation for age assignments based on multiple samples. An exception to the latter is the Libby drainage site representing 38% recession where, as discussed in section 6.1, the standard deviation (0.4 kyr) likely underestimates uncertainty. For that site uncertainty is assumed to be the mean of the internal errors of the two samples (0.8 kyr).

age. Our modeling suggests that West Glacier Lake was also deglaciated between about 14.7 ± 0.7 ka and 14.2 ± 0.6 ka, although a single polished-bedrock sample (SR12-01a) collected ~200 downstream from West Glacier Lake yielded a slightly younger exposure age of 13.7 ± 0.6 ka.

6.1.2. *Comparison to regional records of the LLGM and deglaciation*

Recent work has suggested that throughout the U.S. Rocky Mountains there may have been two intervals of maximum or near-maximum ice extent during the last glaciation (Ward et al., 2009; Leonard et al., 2017a; Licciardi and Pierce, 2018; Schweinsberg et al., 2020; Quirk et al., 2020; Laabs et al., 2020)—one during the global LGM, between 25 ka and 19 ka (Clark et al., 2009) and a subsequent stand of approximately equal extent around 17–16 ka in many areas. However, this does not appear to be the case in all areas. In some areas there is evidence of major recession between about 20 ka and 18 ka, with any subsequent readvance much more limited than the earlier LGM extent (Guido et al., 2007; Ward et al., 2009; Leonard et al., 2017a). As discussed in section 6.1 above, based on the youngest, and most upvalley, boulder age in the Libby Creek glacier terminal moraine complex, it would be possible to argue that while the outermost portion of the complex was likely abandoned near the end of the global LGM, the glacier subsequently either remained at, or readvanced to, a nearly as extensive position, retreating from that position at about 16 ka. However, as also discussed above, we currently feel that a more compelling case can be made for significant post-LLGM recession by about 18 ka, with no evidence of a later significant readvance. More ages from the inner portion of the terminal-moraine complex and from polished-bedrock outcrops immediately upvalley would likely be necessary to resolve this question definitively.

Deglaciation of the Libby Creek drainage was nearly complete by about 14 ka, consistent with observations made in many currently ice-free valleys throughout the Colorado Rocky Mountains (Guido et al., 2007; Ward et al., 2009; Leonard et al., 2017a, 2017b; Tulenko et al., 2020) and elsewhere in the western United States (Munroe and Laabs, 2017; Marcott et al., 2019). The standstills or minor readvances of ice in the French Creek drainage documented by Marcott et al. (2019) indicate, however, that some ice was present in the range until at least as late as 10.5 ± 0.3 ka. While it is possible that one of the moraines dated in French Creek by Marcott et al. (2019) was deposited during a Younger Dryas readvance, such a readvance would have been quite minor compared to the extensive deglaciation that preceded it, and of similar extent to other late glacial and early Holocene events.

6.1.3. *Potential regional, hemispheric, or global forcing of deglaciation*

A good deal of attention has been focused on understanding the primary forcings—global, hemispheric, regional, and/or local—of post-LGM deglaciation in the Rocky Mountains (Young et al., 2011; Leonard et al., 2017a; Tulenko et al., 2020; Laabs et al., 2020), as well as elsewhere in the Western Cordillera of North America and the world (e.g. Ivy-Ochs et al., 2006; Schaefer et al., 2006; Shakun et al., 2015; Marcott et al., 2019; Young et al., 2019; Palacios et al., 2020). Based on the observation that glaciers in the Colorado Sawatch Range appear to have remained close to their LLGM maximum extent until ~16 ka, Young et al. (2011) concluded that primary deglaciation there took place during the Bølling-Allerød interval, implicating North Atlantic forcing as

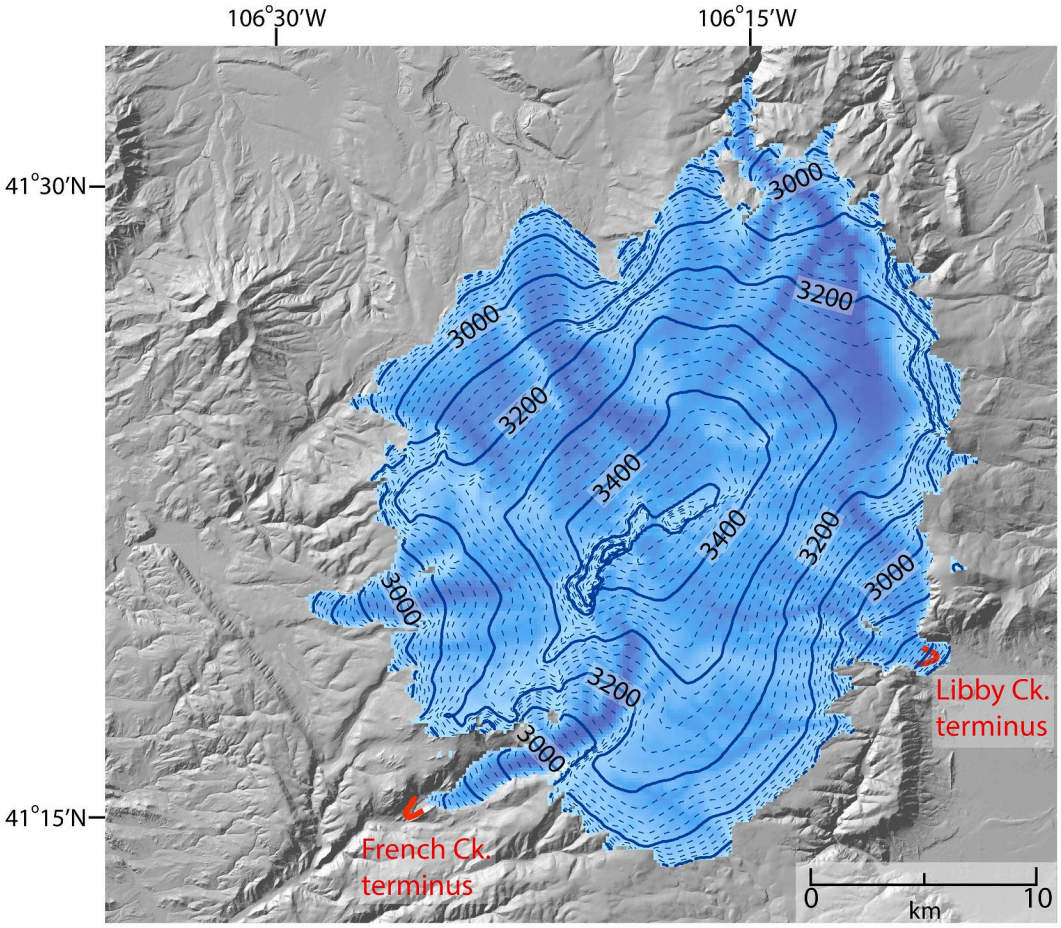

Fig. 7. Simulated Northern Medicine Bow Icefield Complex at the local last glacial maximum, modeled with a year-round temperature depression of 6.0 °C from present and no change from modern precipitation. Simulation is best overall fit to the LLGM terminal positions of the Libby and French Creek drainage glaciers, but slightly overshoots the terminal position of the former and undershoots the terminal position of the latter. Best fit for the Libby Creek terminus alone would involve a 5.9 °C temperature depression with no change in precipitation; best fit for the French Creek terminus alone would involve a 6.1 °C temperature depression. Ice-surface contour interval is 20 m. Shading indicates relative modeled ice thickness—thicker ice is darker. Maximum modeled thickness is 373 m.

a driver for deglaciation in the Rocky Mountains and across the western United States, although the inception of significant deglaciation they documented began about a millennium before the beginning of the Bølling-Allerød interval. More recently, based on additional dating, Tulenko et al. (2020) argue for the same timing of deglaciation in the Sawatch Range, proposing either North Atlantic forcing and/or regional ice-sheet forcing related to the collapse of the saddle connecting the LGM Laurentide and Cordilleran ice sheets. Leonard et al. (2017a), however, pointed out that in some other ranges in the Colorado Rocky Mountains glaciers appear to have begun significant retreat by 18 ka, well before the Bølling-Allerød interval, a pattern also noted by Shakun et al. (2015) at a regional scale across the western United States. Those workers suggested that this earlier initiation of deglaciation likely reflected primarily forcing by atmospheric CO_2, which began its global post-LGM increase ~17ka (Schaefer et al., 2006), possibly combined with somewhat earlier forcing by increasing Northern Hemisphere solar-insolation receipt. Fig. 10a presents ^{10}Be exposure ages for deglaciation, both those in the northern Medicine Bow Mountains from this study and from Marcott et al. (2019), and those available from studies in Colorado (Guido et al., 2007; Briner, 2009; Ward et al., 2009; Dühnforth and Anderson, 2011; Leonard et al., 2017b; Schweinsberg et al., 2016, 2020; Tulenko et al., 2020)—plotted against the normalized length of each glacier (LLGM length = 1.0, complete deglaciation = 0.0), with all ages calculated using PPLSDn production rate and scaling, and error bars including both analytical and production-rate uncertainties. The figure illustrates both the apparent "early" significant retreat of some glaciers, including the Libby Glacier in our preferred interpretation, and the later, ~16 ka, initiation of significant deglaciation elsewhere in the region, which would be consistent with the alternative interpretation of the Libby Glacier sequence.

Fig. 10b shows the LGMR global-mean-temperature evolution since 24 ka, and Fig. 10c–e the record of several proposed forcings through the deglaciation interval. Deglaciation in southern Wyoming and Colorado (Fig. 10a) generally occurred during the time window of sharp rise in global temperatures beginning about 17ka (Fig. 10b), and in most areas deglaciation was completed or nearly completed by about 13 ka. Osman et al. (2021) argue that global warming through this interval was forced by increasing atmospheric CO_2 (Fig. 10c) coupled with feedbacks linked to changing ice sheet albedo. That some Wyoming/Colorado glaciers appear to have undergone significant retreat before 17 ka, however, suggests that increasing northern hemisphere insolation after about 21 ka (Fig. 10d) may have played a role in initiating deglaciation in some areas, as previously suggested by Shakun et al. (2015) and Leonard et al. (2017a). Changes in Atlantic Meridional Overturning Circulation associated with the Bølling-Allerød interval (Fig. 10e) occurred too late to be implicated in the initiation of deglaciation in the central Rocky Mountains. In those areas that have been studied to date, half or more of the total deglacial ice-margin retreat had taken place before the start of the Bølling-Allerød. That said, it is possible that forcing related to North Atlantic circulation changes might have played a role, along with other

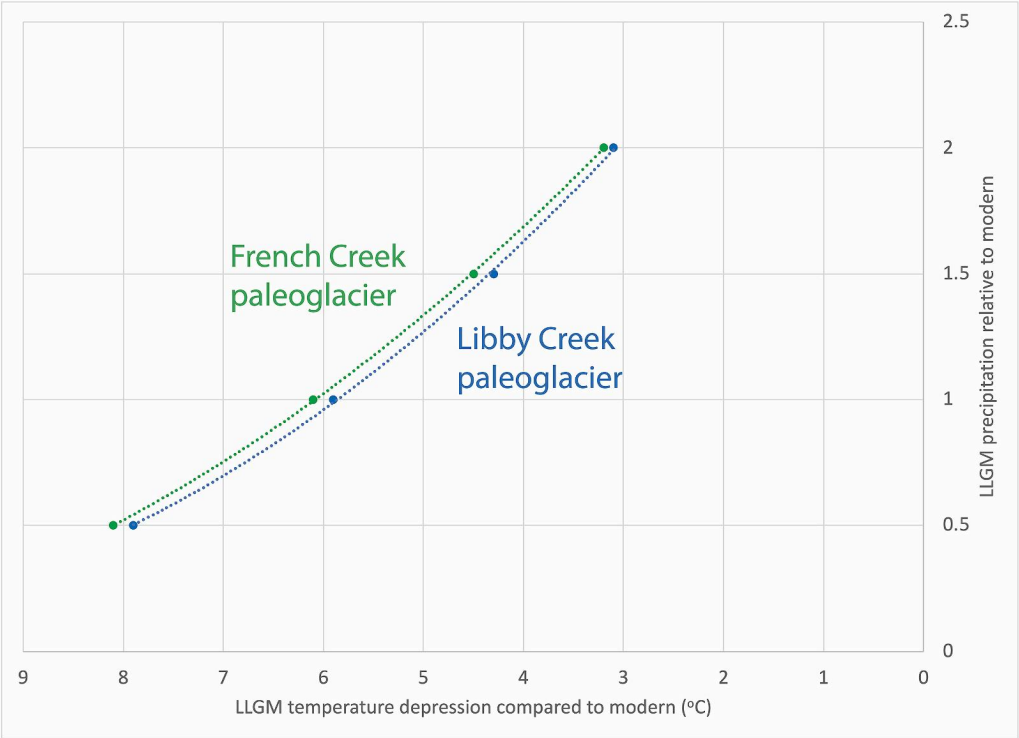

Fig. 8. Combinations of temperature and precipitation change from modern (1971–2000 CE) conditions that could have sustained the Libby Creek (blue) and French Creek (green) paleoglaciers in mass-balance equilibrium at their LLGM extents. Circles indicate individual model simulations; dashed lines are 2nd order polynomial fits to the simulation results for each glacier. (For interpretation of the references to colour in this figure legend, the reader is referred to the Web version of this article.)

forcings, in the final retreat of southern Wyoming and Colorado mountain glaciers, which in most studied areas occurred during the Bølling-Allerød interval.

6.2. *Paleoclimate reconstructions*

Our paleoclimate reconstructions for the LLGM time of 20.7 ± 2.8 ka and for three times during deglaciation, at 18.0 ± 0.8, 14.7 ± 0.4, and 14.2 ± 0.3 ka, are based on calculations of equilibrium conditions. This assumes that the simulated glacier geometries reflected equilibrium mass and flow balances (1) at the time the LLGM moraines were deposited and (2) at the time our dated deglaciation localities were exposed to cosmic radiation. It is commonly argued that the presence of large moraines, such as those that compose the Libby Creek LLGM moraine complex, are indicators of long-term ice-margin stability and thus an approximately steady-state climate to which the glacier has equilibrated, although this assumption has been challenged by some glacier-modeling studies (Roe, 2011; Anderson et al., 2014). The assumption of equilibrium conditions for reconstruction of climate during deglaciation, using ice extent at time intervals defined by the first exposure of bedrock outcrops by retreating ice to assess climate, may be more problematic. Under such conditions, the equilibrium approach is reasonable only if the glacier response is fast relative to the rate of climate change.

We have used two methods to assess the response time of the late Pleistocene Libby Creek glacier and more broadly the Northern Medicine Bow Icefield Complex. In both approaches we make use of our model output to characterize response time. A first approach approximates glacier response time as h/(- $\dot{b}$), where h = either "characteristic" or maximum glacier thickness, and $\dot{b}$ = net balance at the glacier terminus (Jóhannesson et al., 1989a; 1989b; Cuffey and Paterson, 2010). Given this definition and the simulated ice thickness and mass balance for the LLGM Libby Creek glacier over a range of precipitation from 50 to 200% of modern, computed response times range from 41 to 74 years. A second approach to calculating response time is by using model output to determine the apparent "e-folding time" (the time interval necessary to accomplish (1- (1/e)) of the total response to a small climate perturbation—Oerlemans, 2001). Because we modeled the entire icefield complex as a unit, the calculated e-folding time is for the whole complex, based on changes in its volume. Applying a step perturbation of 1.0 °C, we find an e-folding time of 110 years.

Application of model results assuming equilibrium conditions to ice extents defined by exposure ages of bedrock should be interpreted as providing a minimum estimate of the magnitude of climate change forcing deglaciation, as glacier response to changing climate forcing was likely ongoing as the dated samples were exposed. Where the intervals of time over which we are attempting to assess magnitudes and rates of climate change are much longer than the glacier response time, between the LLGM and ~18 ka or between ~18 ka and 14 ka, for example, our assumption of equilibrium conditions likely introduces only minor error. On the other hand, using an equilibrium assumption to infer changes in climate forcing over periods only slightly greater than the glacier response time, such as that between 14.7 ka and 14.2 ka is more problematic and may not be justified. Consequently we do not here consider magnitudes and rates of change in climate forcing based on model output over sub-millennial intervals.

6.2.1. *LLGM climate*

Our model results (Fig. 8) indicate that the LLGM glaciers in the Libby and French Creek drainages could have been sustained with an annual temperature depression from present of about 5.9–6.1 °C, with no change in precipitation, or with temperature depressions of 3.1–3.2 °C or 7.9–8.1 °C with twice or half modern precipitation respectively, with the French Creek glacier in all model simulations requiring slightly more temperature depression at a given precipitation than the Libby Creek glacier. These LLGM temperature-depression estimates are consistent with, or slightly greater than, some regional paleoglacier-based estimates, but are less than temperature-depression estimates from most other glacier-based studies.

Using the same Plummer and Phillips (2003) model, Leonard and colleagues (Gall et al., 2013; Schweinsberg et al., 2016; Leonard et al., 2017b) found that with no precipitation change from present LLGM

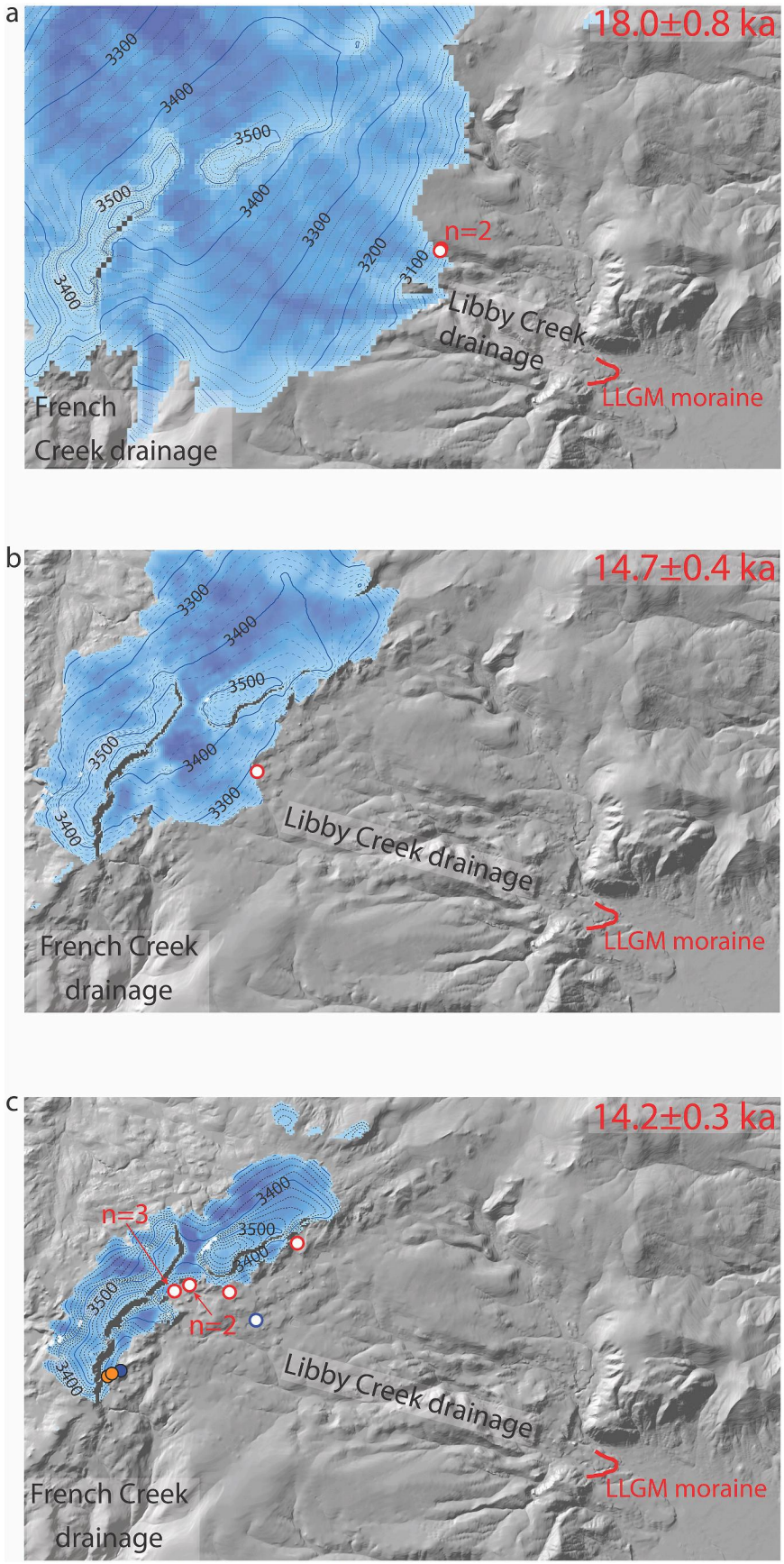

Fig. 9. Simulated deglaciation of southeastern portion of the Northern Medicine Bow Icefield Complex, constrained by surface-exposure ages of moraine and perched boulders and of polished-bedrock outcrops. Locations of boulder samples indicated by filled circles, of polished-bedrock samples by open circles. Red line indicates the outer portion LLGM moraine complex in the Libby Creek drainage. (a) Simulated extent of glaciers at 18.0 ± 0.8 ka constrained by paired polished-bedrock and perched-boulder samples on the left-lateral margin of the Libby Creek glacier. (b) Simulated extent of glaciers at 14.7 ± 0.4 ka constrained by a single polished-bedrock age at the margin of the Libby Creek glacier. (c) Simulated extent of glaciers at 14.2 ± 0.3 ka constrained by polished-bedrock samples in the Libby Creek drainage and moraine-boulder samples in the French Creek drainage (Marcott et al., 2019). Open red circles in panel c indicate location of samples in the 14.2 ± 0.3 ka cluster used to constrain this model, a total of seven samples, with red numbers indicating the number of multiple samples too close together to be plotted separately. Nearly all of these samples are very close to, both within and beyond, the modeled ice margin. In panel c the open blue circle indicates the 14.7 ± 0.4 ka age further downvalley used to constrain the earlier ice margin shown in panel b, and blue circle with black rim the outermost deposit in the French Creek drainage which yielded a mean sample age to 14.5 ± 0.3 ka (Marcott et al., 2019), also located beyond the modeled ice margin here. Orange circles with black rims indicate location of the two younger French Creek deposits that yielded mean ages of 11.5 ± 0.5 ka and 10.5 ± 0.3 ka (Marcott et al., 2019). Both of these deposits are located inside the modeled ice margin. Ice-surface contour interval is 20 m. Shading indicates relative modeled ice thickness—thicker ice is darker. (For interpretation of the references to colour in this figure legend, the reader is referred to the Web version of this article.)

Table 5
Extent of modeled Libby Creek glacier and Northern Medicine Bow Icefields Complex though the deglaciation interval, constrained by locations and ages of ^{10}Be samples in Libby Creek drainage. See Figs. 5 and 6 for location of samples.

Position of Libby drainage glacier margin	Age (ka±1σ uncertainty)	Modeled dT compared to modern[a] (°C)	Approximate equilibrium line altitude (m)	Length of Libby Glacier (km)	Precent of Libby Glacier LLGM length	Area of modeled icefields (km^2)	Precent of modeled area of LLGM icefields
Local last glacial maximum	20.7 ± 2.8	−5.9	3090	14.1	100	568	100
Paired bedrock and erratic samples below Libby Flats	18.0 ± 0.8	−5.0	3210	8.8	62	198	35
Single sample on Libby Flats	14.7 ± 0.4	−4.45	3320	3.5	25	59	10
Multiple samples near base of Snowy Range	14.2 ± 0.3	−4.2	3360	<1	<7	22	4

[a] Assuming no change from modern precipitation. Temperature derpession values are based on model best fits to Libby Creek drainage sample localities.

glaciers in the Front, Sawatch, and Sangre de Cristo ranges in Colorado could have been sustained with temperature depressions ranging from 5.0 to 6.6 °C. In the northern Colorado Front Range, using a coupled degree-day mass-balance and ice-flow model (Kessler et al., 2006), Dühnforth and Anderson (2011) estimated that the LLGM North Boulder Creek glacier could have been sustained with a temperature depression of 4.5–5.8 °C. By contrast, the degree-day model of Brugger and colleagues (Brugger, 2006, 2010; Brugger et al., 2019a, 2019b, 2021) fairly systematically indicates more LLGM temperature depression relative to present than does our modeling, with values ranging from 7.0 to 8.8°C for LLGM glaciers in the Elk, Sawatch, Mosquito, and Sangre de Cristo ranges in central and southern Colorado, assuming no change from modern precipitation. In western Wyoming, Birkel et al. (2012) used the Maine Ice Sheet Model (Fastook and Prentice, 1994), a coupled degree-day mass-balance and flow model, to estimate that at modern precipitation a temperature depression of about 8.5 °C would have been necessary to sustain the LLGM Wind River Range ice cap. Equilibrium-line-altitude based methods (Leonard, 1989, 2007; Brugger and Goldstein, 1999; Refsnider et al., 2009) produce a spread of LLGM temperature-depression estimates for the Wyoming and Colorado Rocky Mountains, ranging from ~6 °C to ~9 °C assuming no change from modern precipitation.

Very few non-glacial proxies in the Wyoming/Colorado area provide quantitative insight into LLGM climate. In an early study based on pollen preserved in proglacial lake sediment in the Colorado Front Range, Legg and Baker (1980) estimated that during the LLGM July daily maximum temperatures may have been ~6 °C colder than today. We are unaware of any other high-altitude non-glacial proxy studies that extend back into the LLGM interval. Two available proxy records from lower-altitude basins suggest much greater late Pleistocene temperature depression. Mears' (1981,1987) work on fossil frost wedges indicated temperature depressions of at least 14 °C, coupled with arid conditions, during the last glaciation. Based on beetle fauna at Lamb Springs in the Denver Basin of Colorado (Fig. 1), Elias (1996) estimated that mean July temperature at ~17.4 ka was 10.4–11.4 °C colder than today, with winter temperatures depressed substantially more. Because both of these studies were in basins at relatively low altitude compared to the glacier sites, comparison of the two types of record depends on assumptions about the stability of altitudinal temperature gradients through the Quaternary.

Climate-model output suggests a range of magnitudes of temperature depression in the northern Medicine Bow region—although in general suggests greater temperature depression than does our glacier modeling. Direct comparisons are made more difficult by differences in resolution and timescales of the publicly available model output and differences in the different models' modern or preindustrial baseline time intervals to which paleotemperatures are compared (see section 4.3 above). Nonetheless the comparisons made here appear to give a fairly clear picture of model-to-model differences in paleotemperature depressions. The LGMR indicates that at about 18.5–17.5 ka mean annual air temperature was about 16.7 °C colder than pre-industrial temperatures in southeastern Wyoming and northern Colorado. Interpolation of TraCE 21ka (Lorenz et al., 2016) output to the eastern flank of the northern Medicine Bow Mountains indicates a mean annual temperature depression of about 11.3 °C at 21–20 ka, the coldest portion of the last 22 kyr in that reconstruction, and interpolation of values from the five "best-fit" PMIP3 climate models (https://pmip3.lsce.ipsl.fr/) yields an ensemble-mean 21 ka temperature on the eastern flank of the Medicine Bows depressed 10.9 °C from preindustrial values, although with a very large model-to-model range (4.4–13.1 °C). All three paleotemperature reconstructions suggest that LGM temperatures were depressed somewhat less during summer (June–August) months, critical months for controlling glacier mass balance in continental environments (Ohmura et al., 1992; Oerlemans, 2001), than during the rest of the year. The LGMR indicates a summer temperature depression of 14.8 °C, TraCE 21ka a summer depression of ~7.4 °C, and the PMIP five-model ensemble a mean summer depression of 9.3 °C (with a model-to-model range of 1.0–13.0 °C). Although smaller than the modeled annual temperature depressions, these LGM summer temperature depressions are generally greater than those indicated by our glacier-model simulations.

Our glacier-model results indicate that for LLGM Northern Medicine Bow Icefield Complex to have been in mass-balance equilibrium with temperature depressions greater than 6.0 ± 1.7 °C, precipitation would need to have been less than modern. As discussed in section 1, most proxy evidence and climate-model output indicate that drier-than-present conditions prevailed in the northern Rocky Mountains at the LGM, wetter-than-modern conditions in the southern Rocky Mountains. An analysis of then-available proxy data and model output by Oster et al. (2015) indicated that at the LGM the transition from a wetter north to a drier south occurred across Colorado, generally to the south of the northern Medicine Bow Mountains. Few LGM precipitation proxies are available for southern Wyoming and northern Colorado. Mears' (1981, 1987) work on fossil frost wedges in the Laramie Basin of southern Wyoming (Fig. 1) indicated dry late Pleistocene conditions, while the pollen work of Legg and Baker (1980) in the Colorado Front Range concluded that LGM conditions there might have been wetter than today. At Little Windy Hill Pond, located within the LLGM ice margin of the Northern Medicine Bow Icefield, Shuman and Serravezza (2017) concluded that lake level was significantly lower than present through the earliest portion of the available record (~17–11 ka), suggesting dry conditions immediately following the LLGM. Climate-model output interpolated to the northern Medicine Bow Mountains is somewhat mixed, with the five "best-fit" PMIP3 models indicating a drying at 21 ka, with mean annual precipitation of 83% of PI (range of individual models—60–106%), fall-through-spring precipitation 81% of PI (range of individual models—50–100%). TraCE 21ka indicates a very slight reduction in annual precipitation at 98% of PI, but an increase in fall through spring precipitation to 119% of PI. While both proxy evidence and climate model output are not definitive, it appears likely that LLGM

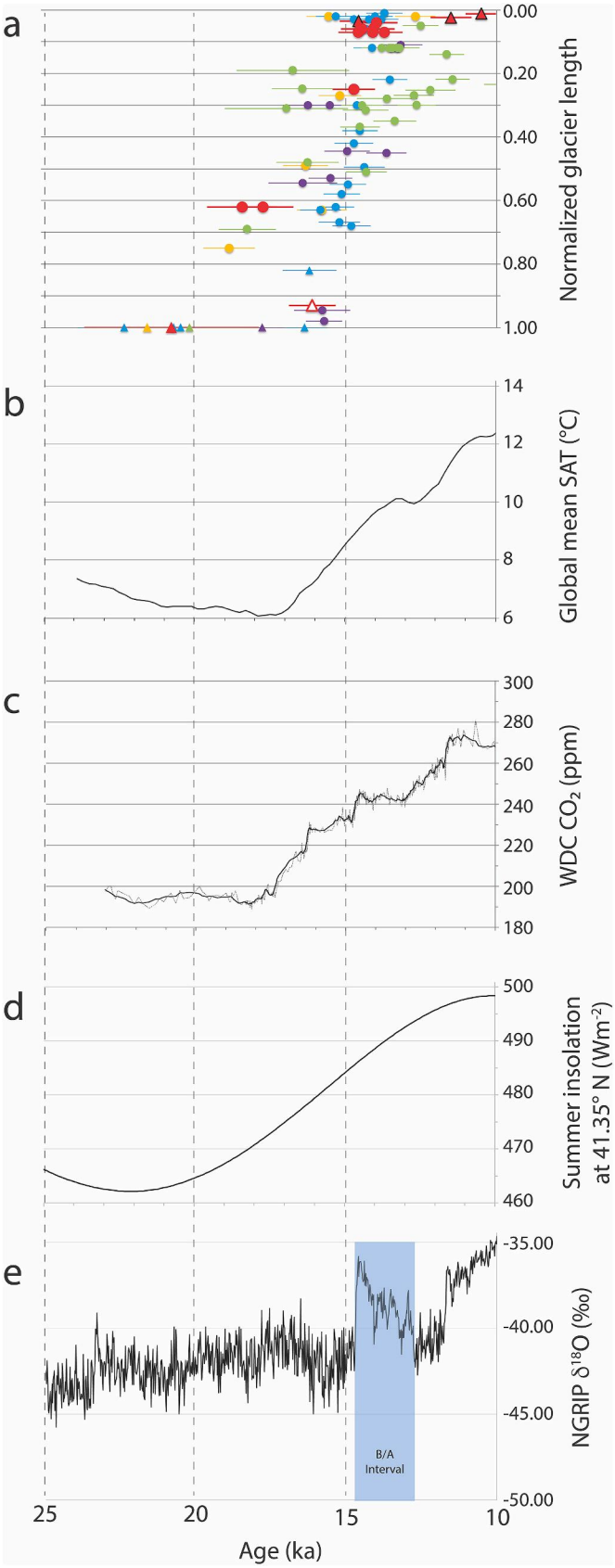

(caption on next column)

Fig. 10. Comparison of the deglaciation record of the Colorado—Wyoming Rocky Mountains to possible forcing mechanisms. (a) Surface-exposure age constraints on deglaciation plotted against normalized position in each glacier valley – with a value 1 corresponding to normalized glacier length at the LLGM and 0 corresponding to complete deglaciation. All plotted age uncertainties reflect both analytical uncertainty and production-rate uncertainty. Ages on moraine boulders are indicated by triangles and are plotted as mean of all ages accepted by the original authors, with plotted uncertainty based on summing in quadrature the 1σ group standard deviation with a 3.78% production-rate uncertainty. Polished-bedrock ages are indicated by circles, with each symbol representing a single age, ±1σ external error. Red symbols indicate ages from the northern Medicine Bow Mountains with ages from French Creek drainage (Marcott et al., 2019) shown with a black outline, those from Libby Creek drainage (this study) with no outline. The open red triangle indicates age of the single boulder on the inner portion of the Libby Creek moraine complex that we believe to be influenced by post-deposition shielding. Smaller symbols represent ages reported previously in Colorado, with all ages recalculated to the PPLSDn production rate and scaling. Blue symbols are samples from the Sawatch Range (Briner, 2009; Schweinsberg et al., 2016, 2020; Tulenko et al., 2020); purple symbols from the Sangre de Cristo Mountains (Leonard et al., 2017b); green from the Front Range (Ward et al., 2009; Dühnforth and Anderson, 2011); yellow from the San Juan Mountains (Guido et al., 2007). (b) Global mean surface air temperature (Osman et al., 2021) (c) Summer (June–July–August) insolation for 41.35°N (Calculated using web calculator http://vo.imcce.fr/insola/earth/online/earth/online/index.php; based on Laskar et al., 2004). (d) Atmospheric CO_2 from West Antarctic Ice Sheet Divide Ice Core (WDC)—plotted with five-point running mean (Marcott et al., 2014); (e) $\delta^{18}O$ record from North Greenland Ice Core Project (NGRIP) core (Members N. G.R.I.P., 2004); a proxy for possible North Atlantic forcing. Blue shading indicates the Bølling/Allerød warm interval. Vertical dashed lines are at 20 and 15 ka. (For interpretation of the references to colour in this figure legend, the reader is referred to the Web version of this article.)

precipitation in the northern Medicine Bow Mountains was somewhat less than the PI. Coupled with our glacier-model results, this therefore suggests an LLGM temperature depression of somewhat greater than 6 °C.

6.2.2. *Deglaciation climate*

Our modeling suggests that only modest amounts of temperature rise triggered the nearly complete deglaciation of the range between ~20.7 ± 2.8 ka and 14.2 ± 0.3 ka. Assuming that there was no change in precipitation, a rise of only ~0.9 °C would have sufficed to drive significant deglaciation of the Libby Creek drainage by 18.0 ± 0.8 ka, and a further rise of ~0.8 °C by 14.2 ± 0.3 ka would have resulted in nearly complete deglaciation. Following 14.2 ± 0.3 ka, an additional rise in temperature of 4.2 °C to present conditions, resulting in total deglaciation of the range, would have occurred over an unknown time interval. As discussed in section 6.2 above, given concern about the validity of applying equilibrium assumptions to glacier response to relatively short-term changes in climate forcing, we do not consider the 14.7 ka model results separately from the 18.0 ka and 14.2 ka results. As discussed in section 6.2.1, while there is uncertainty about precipitation during the LGM, it seems probable that conditions at that time were somewhat drier than present. Evidence from Little Windy Hill Pond in the northern Medicine Bow Mountains indicates that the major post-LGM increase in lake level did not occur until ~11 ka, coincident with rises in many lakes in Wyoming and Colorado region (Pribyl and Shuman, 2014; Schuman and Serravezza, 2017). This change in lake level postdates the main period of deglaciation, suggesting that ice retreat was driven primarily by temperature change.

In three valleys in the Colorado Rocky Mountains, similar combinations of upvalley exposure-age data and numerical glacier modeling allow comparison to our Medicine Bow paleotemperature results. Although one of the studies (Leonard et al., 2017b) examined possible effect of precipitation changes during deglaciation, here we discuss only temperature-change forcing of deglaciation. Fig. 11 summarizes the general pattern of simulated post-LGM temperature rise during and

following the period of deglaciation in the four valleys, assuming that precipitation did not change significantly through the interval in any of the areas. In the North Boulder Creek valley of the Colorado Front Range, Dühnforth and Anderson (2011) found that deglaciation was accomplished by an approximately 2.0 °C temperature rise between the LLGM (~24–18 ka) and ~14 ka and a subsequent 1.0 °C temperature rise between ~14 and ~12 ka, by which time the valley was almost entirely ice free (original ages ^{10}Be ages recalculated by Laabs et al., 2020). Subsequent to ~12 ka temperature has risen 1.5–2.8 °C. Work in the Lake Creek valley in the Sawatch Range of central Colorado (Schweinsberg et al., 2016, 2020; Leonard et al., 2017a, unpublished data – early ^{10}Be ages recalculated by Schweinsberg et al., 2020) indicates a temperature rise of 0.8 °C from ~20.6 ka to ~15.2 ka which resulted in initial deglaciation. The main deglaciation of the valley took place rapidly in response to a subsequent rise of ~2.3 °C between ~15.2 and ~13.7 ka. Subsequent to ~13.7 ka temperature has risen another ~2.3 °C. In the Willow Creek valley in the Sangre de Cristo Mountains of southern Colorado, Leonard et al. (2017b–^{10}Be ages recalculated by Laabs et al., 2020) concluded that, assuming no changes in precipitation, temperature would have risen by about 2.5 °C from ~17.7 ka (and primarily after 15.7 ka) to ~13.2 ka, resulting in nearly complete deglaciation of the valley, followed by an additional rise of ~2.5 °C to present.

Nearly total deglaciation in all four areas required only 1.6–3.1 °C of post-LLGM temperature rise, and was accomplished in all four areas by 14–12 ka. After that time, subsequent temperature rises of 1.5–4.6 °C resulted loss of all glaciers in three of the areas, although limited glacier ice still remains in the North Boulder Creek drainage.

6.3. Glacier sensitivity

It is initially somewhat surprising that the icefield complex in the northern Medicine Bow Mountains disappeared nearly completely in response to relatively small climate change. A temperature rise of only about 1.7 °C, assuming no change in precipitation, resulted in a loss of about 96% of the total area are of the complex, with only about 22 km^2 remaining of the ~600 km^2 LLGM icefield complex (Table 5). The icefield complex for the most part occupied a broad, relatively low-relief upland. As long as the majority of the upland was above the glacier equilibrium line altitudes (ELAs), the icefield was extensive and fed major outlet valley glaciers. However, even a small rise of ELAs could raise them above much of the upland surface, leading to extensive deglaciation. So, for example, at the LLGM when the ELA was ~3090 m, ~49 km^2 of the subglacial topography of the Libby Creek drainage was above the ELA, including much of the low-relief Libby Flats surface. The subsequent 270 m ELA rise to 3360 m that occurred by 14.2 ± 0.3 ka put nearly all of that surface below the ELA, leaving only about 2.8 km^2 of the topography above the ELA. As a result of this relatively small ELA rise, glacier extent in the Libby Creek drainage was reduced from ~103 km^2 to ~3.6 km^2.

7. Conclusions

The chronology we have developed for the east side of the of the northern Medicine Bow Mountains indicates that significant deglaciation there likely began prior to 18 ka, and that deglaciation was nearly complete by about 14 ka. Deglaciation was likely initiated, possibly as early as ~21 ka, by a rise in summer insolation, and after ~17 ka additionally forced by warming related to increased atmospheric CO_2 and changing ice-sheet albedo. Changes in North Atlantic circulation may also have contributed, but only during the final phases of deglaciation, as by early in the Bølling-Allerød interval, the glacier in the Libby Creek drainage has receded to only about 25% of its LLGM length and the entire icefield complex was reduced to only 10% of its LLGM area. Combining this geochronology with modeling results, however, indicates that while warming between the LLGM and the mid-Bølling-Allerød resulted in almost complete deglaciation of the range, it may have involved only about 30% of the total LLGM-to-modern warming. The remainder of that warming occurred later, after the near-total disappearance of ice – likely in good part during the later phases of the Bølling-Allerød interval and the subsequent transition to the Holocene. Because the initial phases of post-LLGM warming were sufficient to raise equilibrium lines above nearly all of the upland plateau of the northern Medicine Bow Mountains, glaciers disappeared almost entirely at that time. Consequently, evidence of later warming, which our modeling indicates was of greater magnitude that the initial warming, is

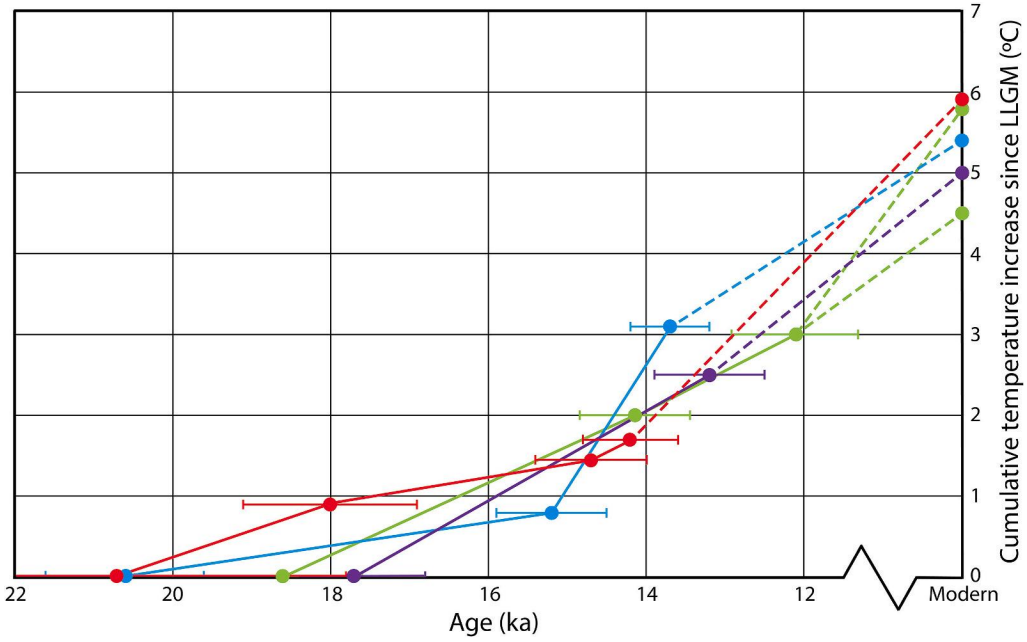

Fig. 11. Pattern of temperature rise in the Wyoming/Colorado Rocky Mountains following the local last glacial maximum, based on numerical modeling of paleoglaciers. Lines indicate linear interpolations between times (indicated by circles) for which paleoclimate was modeled from dated ice extent. Lines are dashed either to reflect different interpretations given by the original authors and/or the fact that the time when temperature rose to approximately modern levels is not known. Error bars indicate 1σ uncertainty on ages, calculated including production-rate uncertainty. Red symbols indicate model results from the current study in the northern Medicine Bow Mountains, blue symbols from the Sawatch Range of Colorado (Schweinsberg et al., 2016; Leonard et al., 2017a, unpublished data), green symbols from the Colorado Front Range (Dühnforth and Anderson., 2011), purple symbols from the Colorado Sangre de Cristo Mountains (Leonard et al., 2017b). (For interpretation of the references to colour in this figure legend, the reader is referred to the Web version of this article.)

not well preserved in the range.

Our modeling indicates that LLGM glaciation in the northern Medicine Bow Mountains was forced by relatively modest temperature depression with respect to present conditions, only about 6.0 ± 1.7 °C if LLGM precipitation were the same as present, or between ~3 and ~8 °C if LLGM precipitation was between twice and half modern, respectively. As most proxy evidence and climate model output suggest somewhat reduced precipitation at the LLGM, a temperature depression of somewhat greater (i.e., colder) than 6.0 ± 1.7 °C appears likely. These estimates are consistent with other paleoglacier-based estimates of regional LGM climate derived using the same model we have used in this study and using some other glacier models and proxies. They do, however, imply less change from modern conditions than is suggested by yet other glacier models, other proxies, and many global climate model simulations. Resolving these differences is important both in understanding regional climate history and in improving performance of glacier-based paleoclimate modeling, and is a focus of ongoing research.

Declaration of competing interest

The authors declare that they have no known competing financial interests or personal relationships that could have appeared to influence the work reported in this paper.

Data availability

Data will be made available on request.

Acknowledgements

Jessica Treanton, Vivian Spiess, Zach Snyder, Alex Robertson, John Collis, and Dan Wolf assisted in field sample collection for cosmogenic exposure dating, and Jessica Treanton, Vivian Spiess, Ryan Gall, Laura Best, Charles Krueger, Elizabeth (Huss) Sanguinito, Brendon Quirk, Alec Spears, Douglas Steen, Katherine Truong, and Jessica Lam assisted in processing the samples in the lab at SUNY-Geneseo. Ryan Kroner contributed to modeling work. J. Batbaatar's review of the manuscript led us to reconsider and improve our understanding and discussion of exposure-age uncertainties. We thank Medicine Bow National Forest for permitting us to collect samples in a popular hiking and camping area. Financial support was provided to EML, BJCL and MAP by the United States National Science Foundation [NSF/GLD 1024838 and NSF/GLD 1024852] and to BTM by the Colorado College Department of Geology Patricia Buster Research Scholarship Fund.

Appendix A. Supplementary data

Supplementary data to this article can be found online at https://doi.org/10.1016/j.qsa.2023.100109.

References

Anderson, L.S., Roe, G.H., Anderson, R.S., 2014. The effects of interannual climate variability on the moraine record. Geology 42, 55–58. https://doi.org/10.1130/G34791.1.

Applegate, P.J., Urban, N.M., Laabs, B.J.C., Keller, K., Alley, R.B., 2010. Modeling the statistical distributions of cosmogenic exposure dates from moraines. Geosci. Model Dev. (GMD) 3, 293–307. http://gmd.copernicus.org/articles/3/293/2010/.

Atwood Jr., W.W., 1937. Records of Pleistocene glaciers in the medicine Bow and park ranges. J. Geol. 45, 113–140.

Balco, G., 2011. Contributions and unrealized potential contributions of cosmogenic-nuclide exposure dating to glacier chronology, 1990–2010. Quat. Sci. Rev. 30, 3–27. https://doi.org/10.1016/j.quascirev.2010.11.003.

Balco, G., Schaefer, J.M., 2006. Cosmogenic-nuclide and varve chronologies for the deglaciation of southern New England. Quat. Geochronol. 1, 15–28. https://doi.org/10.1016/j.quageo.2006.06.14.

Balco, G., Stone, J.O., Lifton, N.A., Dunai, T.J., 2008. A complete and easily accessible means of calculating surface exposure ages or erosion rates from 10Be and 26Al measurements. Quat. Geochronol. 3, 174–195. https://doi.org/10.1016/j.quageo.2007.12.001.

Barrows, T.T., Stone, J.O., Fifield, L.K., Cresswell, R.G., 2002. The timing of the last glacial maximum in Australia. Quat. Sci. Rev. 21, 159–173.

Bartlein, P.J., Hostetler, S.W., 2004. Modeling paleoclimates. Dev. Quat. Sci. 1, 565–584. https://doi.org/10.1016/S1571-0866(03)01027-3.

Birkel, S.D., Putnam, A.E., Denton, G.H., Koons, P.O., Fastook, J.L., Putnam, D.E., Maasch, K.A., 2012. Climate inferences from a glaciological reconstruction of the late Pleistocene Wind River ice cap, Wind River range, Wyoming. Arctic Antarct. Alpine Res. 44, 265–276. https://doi.org/10.1657/1938-4246-44.3.265.

Blackstone, D.L., 1987. Northern Medicine Bow Mountains, Wyoming; revision of structural geology, northeast flank. Rocky Mt. Geol. 25, 1–9.

Blackwelder, E., 1915. Post-Cretaceous history of the mountains of central western Wyoming. J. Geol. 23, 193–217.

Borchers, B., Marrero, S., Balco, G., Caffee, M., Goehring, B., Lifton, N., Nishiizumi, K., Phillips, F., Schaefer, J., Stone, J., 2016. Geological calibration of spallation production rates in the CRONUS-Earth project. Quat. Geochronol. 31, 188–198. https://doi.org/10.1016/j.quageo.2015.01.009.

Briner, J.P., 2009. Moraine pebbles and boulders yield indistinguishable ^{10}Be ages: a case study from Colorado, USA. Quat. Geochronol. 4, 299–305. https://doi.org/10.1016/j.quageo.2009.02.010.

Briner, J.P., Kaufman, D.S., Manley, W.F., Finkel, R.C., Caffee, M.W., 2005. Cosmogenic exposure dating of late Pleistocene moraine stabilization in Alaska. Geol. Soc. Am. Bull. 117, 1108–1120. https://doi.org/10.1130/B25649.1.

Brugger, K.A., 2006. Late Pleistocene climate inferred from the reconstruction of the Taylor River glacier complex, southern Sawatch Range, Colorado. Geomorphology 75, 318–329. https://doi.org/10.1016/j.geomorph.2005.07.020.

Brugger, K.A., 2010. Climate in the southern Sawatch range and Elk mountains, Colorado, USA, during the last glacial maximum: inferences using a simple degree-day model. Arctic Antarct. Alpine Res. 42, 164–178. https://doi.org/10.1657/1938-4246-42.2.164.

Brugger, K.A., Goldstein, B.S., 1999. Paleoglacier reconstruction and late-Pleistocene equilibrium-line altitudes, southern Sawatch Range, Colorado. In: Mickelson, D.M., Attig, J.W. (Eds.), Glacial Processes Past and Present, vol. 337. Geological Society of America Special Paper, pp. 103–112.

Brugger, K.A., Laabs, B., Reimers, A., Benson, N., 2019a. Late Pleistocene glaciation in the Mosquito range, Colorado: chronology and climate. J. Quat. Sci. 34, 187–202. https://doi.org/10.1002/jqs.3090.

Brugger, K.A., Ruleman, C.A., Caffee, M.W., Mason, C.C., 2019b. Climate during the last glacial maximum in the northern Sawatch range, Colorado. Quaternary 2, 36. https://doi.org/10.3390/quat2040036.

Brugger, K.A., Leonard, E.M., Refsnider, K.A., Dolan, P., 2021. Climate on the blanca massif, Sangre de Cristo mountains, Colorado, during the last glacial maximum. Quaternary 4, 27. https://doi.org/10.3390/quat4030027.

Brunelle, A., Minckley, T.A., Lips, E., Burnett, P., 2013. A record of late-glacial/Holocene environmental change from a high-elevation site in the Intermountain West, U.S.A. J. Quat. Sci. 28, 103–112. https://doi.org/10.1002/jqs.2600.

Carter, V.A., Brunelle, A., Minckley, T.A., Dennison, E., Power, M.J., 2013. Regionalization of fire regimes in the Central Rocky Mountains, USA. Quat. Res. 80, 406–416. https://doi.org/10.1016/j.qres.2013.07.009.

Clark, P.U., Dyke, A.S., Shakun, J.D., Carlson, A.E., Clark, J., Wohlfarth, B., Mitrovica, J. X., Hostetler, S.W., McCabe, A.M., 2009. The Last Glacial Maximum. Science 325, 710–714. https://doi.org/10.1126/science.1172873.

COHMAP Members, 1988. Climatic changes of the last 18,000 years: observations and model simulations. Science 241, 1043–1052.

Cuffey, K.M., Paterson, W.S.B., 2010. The Physics of Glaciers, fourth ed. Butterworth-Heinemann/Elsevier, p. 693.

Davis, P.T., Davis, R.B., 1980. Interpretation of minimum-limiting radiocarbon dates for deglaciation of Mt. Katahdin area, Maine. Geology 8, 396–400.

Dühnforth, M., Anderson, R.S., 2011. Reconstructing the glacial history of Green Lakes Valley, North Boulder Creek, Colorado Front Range. Arctic Antarct. Alpine Res. 43, 527–542. https://doi.org/10.1657/1938-4246-43.4.527.

Elias, S.A., 1996. Late Pleistocene and Holocene seasonal temperatures reconstructed from fossil beetle assemblages in the Rocky Mountains. Quat. Res. 46, 311–318.

Fastook, J.L., Prentice, M., 1994. A finite-element model of Antarctica: sensitivity test for meteorological mass-balance relationship. J. Glaciol. 40, 167–175.

Gall, R.D., Leonard, E.M., Plummer, M.A., Laabs, B.J.C., 2013. Numerical modeling of the Middle Boulder Creek paleoglacier in the Colorado Front Range: insights into LGM paleoclimate and post-LGM rates of climate change. Geol. Soc. Am. Annu. Meet. Abstr. 45, 346.

Guido, Z.G., Ward, D.J., Anderson, R.S., 2007. Pacing the post–Last Glacial Maximum demise of the Animas Valley glacier and the San Juan Mountain ice cap, Colorado. Geology 35, 739–742. https://doi.org/10.1130/G23596A.1.

Heyman, J., Applegate, P.J., Blomdin, R., Gribenski, N., Harbor, J.M., Stroeven, A.P., 2016. Boulder height–exposure age relationships from a global glacial ^{10}Be compilation. Quat. Geochronol. 34, 1–11. https://doi.org/10.1016/j.quageo.2016.03.002.

Hoffman, M.J., Fountain, A.G., Achuff, J.M., 2007. 20th-century variations in area of cirque glaciers and glacierets, Rocky Mountain National Park, Rocky Mountains, Colorado, USA. Ann. Glaciol. 46, 349–354. https://doi.org/10.3189/172756407782871233.

Houston, R.S., Karlstrom, K.E., 1992. Geologic map of Precambrian metasedimentary rocks of the Medicine Bow Mountains, Albany and Carbon counties, Wyoming. U.S. Geol. Surv. Misc. Invest. Ser. Map I 2280, 1–50, 000.

Hudson, A.M., Hatchett, B.J., Quade, J., Boyle, D.P., Bassett, S.D., Ali, G., De los Santos, M.G., 2019. North-south dipole in winter hydroclimate in the western United States during the last deglaciation. Sci. Rep. 9, 1–12. https://doi.org/10.1038/s41598-019-41197-y.

Hutter, K., 1983. Theoretical Glaciology: Material Science of Ice and the Mechanics of Glaciers and Ice Sheets. Reidel, Dordrecht, p. 510p.
Ibarra, D.E., Oster, J.L., Winnick, M.J., Caves Rugenstein, J.K., Byrne, M.P., Chamberlain, C.P., 2018. Warm and cold wet states in the western United States during the Pliocene–Pleistocene. Geology 46, 355–358. https://doi.org/10.1130/G39962.1.
Ivy-Ochs, S., Kerschner, H., Reuther, A., Maisch, M., Sailer, R., Schaefer, J., Kubik, P.W., Synal, H.-A., 2006. The timing of glacier advances in the northern European Alps based on surface exposure dating with cosmogenic ^{10}Be, ^{26}Al, ^{36}Cl, and ^{21}Ne. Geol. Soc. Am. Spec. Pap. 415, 43. https://doi.org/10.1130/2006.2415(04.
Jóhannesson, T., Raymond, C., Waddington, E., 1989a. A simple method for determining the response time of glaciers. In: Orlemans, J. (Ed.), Glacier Fluctuations and Climate Change. Kluwer, Dordrecht, Netherlands, pp. 343–352.
Jóhannesson, T., Raymond, C., Waddington, E., 1989b. Timescale for adjustment of glaciers to changes in mass balance. J. Glaciol. 35, 355–369.
Karlstrom, K.E., Flurkey, A.J., Houston, R.S., 1983. Stratigraphy and depositional setting of the Proterozoic Snowy Pass Supergroup, southeastern Wyoming: Record of an early Proterozoic Atlantic-type cratonic margin. Geol. Soc. Am. Bull. 94, 1257–1274.
Kessler, M.A., Anderson, R.S., Stock, G.M., 2006. Modeling topographic and climatic control of east-west asymmetry in Sierra Nevada glacier length during the Last Glacial Maximum. J. Geophys. Res.: Earth Surf. 111, F02002 https://doi.org/10.1029/2005JF000365.
Kohl, C.P., Nishiizumi, K., 1992. Chemical isolation of quartz for measurement of in-situ-produced cosmogenic nuclides. Geochem. Cosmochim. Acta 56, 3583–3587.
Kutzbach, J., Gallimore, R., Harrison, S., Behling, P., Selin, R., Laarif, F., 1998. Climate and biome simulations for the past 21,000 years. Quat. Sci. Rev. 17, 473–506.
Laabs, B.J.C., Plummer, M.A., Mickelson, D.M., 2006. Climate during the Last Glacial Maximum in the Wasatch and southern Uinta Mountains inferred from glacier modeling. Geomorphology 75, 300–317. https://doi.org/10.1016/j.geomorph.2005.07.026.
Laabs, B.J., Munroe, J.S., Best, L.C., Caffee, M.W., 2013. Timing of the last glaciation and subsequent deglaciation in the Ruby Mountains, Great Basin, USA. Earth Planet Sci. Lett. 361, 16–25. https://doi.org/10.1016/j.epsl.2012.11.018.
Laabs, B.J.C., Licciardi, J.M., Leonard, E.M., Marchetti, D.W., Munroe, J.S., 2020. Updated cosmogenic chronologies of Pleistocene mountain glaciation in the western United States and associated paleoclimate inferences. Quat. Sci. Rev. 242 https://doi.org/10.1016/j.quascirev.2020.106427.
Laskar, J., Robutel, P., Joutel, F., Gastineau, M., Correia, A.C.M., Levrard, B., 2004. A long term numerical solution for the insolation quantities of the Earth. Astron. Astrophys. 428, 261–285. https://doi.org/10.1051/0004-6361:20041335.
Legg, T.E., Baker, R.G., 1980. Palynology of Pinedale sediments, Devlins Park, Boulder County, Colorado. Arct. Alp. Res. 12, 319–333.
Leonard, E.M., 1989. Climatic change in the Colorado Rocky Mountains: estimates based on modern climate at late Pleistocene equilibrium lines. Arct. Alp. Res. 21, 245–255.
Leonard, E.M., 2007. Modeled patterns of Late Pleistocene glacier inception and growth in the Southern and Central Rocky Mountains, USA: sensitivity to climate change and paleoclimatic implications. Quat. Sci. Rev. 26, 2152–2166. https://doi.org/10.1016/j.quascirev.2007.02.013.
Leonard, E.M., Plummer, M.A., Carrara, P.E., 2014. Numerical modeling of the Snowmass Creek paleoglacier, Colorado: implications for climate in the Rocky Mountains during the Bull Lake glaciation (MIS 6). Quat. Res. 82, 533–541. https://doi.org/10.1016/j.yqres.2014.03.001.
Leonard, E.M., Laabs, B.J.B., Schweinsberg, A.D., Russell, C.M., Briner, J.B., Young, N.E., 2017a. Deglaciation of the Colorado Rocky Mountains following the Last Glacial Maximum. Cuadernos Invest. Geogr. 43, 497–526. https://doi.org/10.18172/cig.3234.
Leonard, E.M., Laabs, B.J., Plummer, M.A., Kroner, R.K., Brugger, K.A., Spiess, V.M., Refsnider, K.A., Xia, Y., Caffee, M.W., 2017b. Late Pleistocene glaciation and deglaciation in the Crestone Peaks area, Colorado Sangre de Cristo Range – chronology and paleoclimate. Quat. Sci. Rev. 158, 127–144 doi:j.quascirev.2016.11.024.
Leonard, E.M., Laabs, B.J.C., Robertson, A., Plummer, M.A., Ibarra, D.E., Caffee, M.W., 2023. Late Pleistocene glaciation in the southernmost Sangre de Cristo Mountains, New Mexico – chronology and paleoclimate. Quat. Sci. Adv. 9, 100070 https://doi.org/10.1016/j.qsa.2023.100070.
Licciardi, J.M., Pierce, K.L., 2018. History and dynamics of the Greater Yellowstone Glacial System during the last two glaciations. Quat. Sci. Rev. 200, 1–33. https://doi.org/10.1016/j.quascirev.2018.08.027.
Lifton, N., Sato, T., Dunai, T.J., 2014. Scaling *in situ* cosmogenic nuclide production rates using analytical approximations to atmospheric cosmic-ray fluxes. Earth Planet Sci. Lett. 386, 149–160. https://doi.org/10.1016/j.epsl.2013.10.052.
Lifton, N., Caffee, M., Finkel, R., Marrero, S., Nishiizumi, K., Phillips, F.M., Goehring, B., Gosse, J., Stone, J., Schaefer, J., Theriault, B., 2015. *In situ* cosmogenic nuclide production rate calibration for the CRONUS-Earth project from Lake Bonneville, Utah, shoreline features. Quat. Geochronol. 26, 56–69. https://doi.org/10.1016/j.quageo.2014.11.002.
Lisiecki, L.E., Raymo, M.E., 2005. A Pliocene-Pleistocene stack of 57 globally distributed benthic δ18O records. Paleoceanography 20, 1–17. https://doi.org/10.1029/2004PA001071.
Lora, J.M., Ibarra, D.E., 2019. The North American hydrological cycle through the last deglaciation. Quat. Sci. Rev. 226 https://doi.org/10.1016/j.quascirev.2019.105991.
Lora, J.M., Mitchell, J.L., Tripati, A.E., 2016. Abrupt reorganization of North Pacific and western North American climate during the last deglaciation. Geophys. Res. Lett. 43 (11) https://doi.org/10.1002/2016GL071244, 796-11,804.
Lora, J.M., Mitchell, J.L., Risi, C., Tripati, A.E., 2017. North Pacific atmospheric rivers and their influence on western North America at the Last Glacial Maximum. Geophys. Res. Lett. 44, 1051–1059, 2016GL071541.
Lorenz, D.J., Nieto-Lugilde, D., Blois, J.L., Fitzpatrick, M.C., Williams, J.W., 2016. Downscaled and debiased climate simulations for North America from 21,000 years ago to 2100AD. Sci. Data 3, 160048. https://doi.org/10.1038/sdata.2016.48.
McCallum, M.E., 1962. Glaciation of Libby Creek Canyon, East Flank of Medicine Bow Mountains, Southeastern Wyoming. Univ. Wyoming Contrib. Geol. 1, 21–29.
Marcott, S.A., Bauska, T.K., Buizert, C., Steig, E.J., Rosen, J.L., Cuffey, K.M., Fudge, T.J., Severinghaus, J.P., Ahn, J., Kalk, M.L., McConnell, J.R., 2014. Centennial-scale changes in the global carbon cycle during the last deglaciation. Nature 514, 616–619. https://doi.org/10.1038/nature13799.
Marcott, S.A., Clark, P.U., Shakun, J.D., Brook, E.J., Davis, P.T., Caffee, M.W., 2019. ^{10}Be age constraints on latest Pleistocene and Holocene cirque glaciation across the western United States. npj Clim. Atmos. Sci. 2, 1–7. https://doi.org/10.1038/s41612-019-0062-z.
Mears, B., 1981. Periglacial wedges and the late Pleistocene environment of Wyoming's intermontane basins. Quat. Res. 15, 171–198.
Mears, B.J., 1987. Late Pleistocene periglacial wedge sites in Wyoming. Geol. Surv. Wyoming Memoir 3, 77p.
Mears, B., 2001. Glacial records in the Medicine Bow Mountains and Sierra Madre of southern Wyoming and adjacent Colorado, with a traveler's guide to their sites. Wyoming State Geological Survey Publ. Inf. Circ. 41, 26p.
Members N.G.R.I.P., 2004. High-resolution record of Northern Hemisphere climate extending into the last interglacial period. Nature 431, 147–151. https://doi.org/10.1038/nature02805.
Mensing, S., Korfmacher, J., Minckley, T.A., Musselman, R., 2011. A 15,000-year record of vegetation and climate change from a tree line lake in the Rocky Mountains, Wyoming, U.S.A. Holocene 22, 739–748. https://doi.org/10.1177/0959683611430339.
Minckley, T.A., 2014. Postglacial vegetation history of southeastern Wyoming, U.S.A. Rocky Mt. Geol. 49, 61–74. https://doi.org/10.2113/gsrocky.49.1.61.
Minckley, T.A., Shriver, R.K., Shuman, B., 2012. Resilience and regime change in a southern Rocky Mountain ecosystem during the past 17 000 years. Ecol. Monogr. 82, 49–68 jstor.org/stable/23206684.
Morrill, C., Lowry, D.P., Hoell, A., 2018. Thermodynamic and dynamic causes of pluvial conditions during the last glacial maximum in Western North America. Geophys. Res. Lett. 45, 335–345. https://doi.org/10.1002/2017GL075807.
Munroe, J.S., Laabs, B.J., 2017. Combining radiocarbon and cosmogenic ages to constrain the timing of the last glacial-interglacial transition in the Uinta Mountains. Utah, USA. Geol. 45, 171–174. https://doi.org/10.1130/G38156.1.
Muzikar, P., Elmore, D., Granger, D.E., 2003. Accelerator mass spectrometry in geologic research. Geol. Soc. Am. Bull. 115, 643–654, 10.1130/0016-7606(2003)115<0643:AMSIGR>2.0.CO;2.
Nishiizumi, K., Imamura, M., Caffee, M.W., Southon, J.R., Finkel, R.C., McAninch, J., 2007. Absolute calibration of ^{10}Be AMS standards. Nucl. Instrum. Methods Phys. Res. Sect. B Beam Interact. Mater. Atoms 258, 403–413. https://doi.org/10.1016/j.nimb.2007.01.297.
Oerlemans, J., 2001. Glaciers and Climate Change. Balkema Publishers, Lisse, p. 148p.
Ohmura, A., Kasser, P., Funk, M., 1992. Climate at the equilibrium line of glaciers. J. Glaciol. 38, 397–411.
Osman, M.B., Tierney, J.E., Zhu, J., Tardif, R., Hakim, G.J., King, J., Poulsen, C.J., 2021. Globally resolved surface temperatures since the Last Glacial Maximum. Nature 599, 239–244. https://doi.org/10.1038/s41586-021-03984-4.
Oster, J.L., Ibarra, D.E., 2019. Glacial hydroclimate of western North America: insights from proxy-model comparison and implications for Lake Bonneville. In: Lund, W.R., McKean, A.P., Bowman, S.D. (Eds.), Proceedings Volume: 2018 Lake Bonneville Geologic Conference and Short Course, October 3-6, 2018, vol. 170. Utah Geological Survey Miscellaneous Publication.
Oster, J.L., Ibarra, D.E., Winnick, M.J., Maher, K., 2015. Steering of westerly storms over western North America at the Last Glacial Maximum. Nat. Geosci. 8, 201–205. https://doi.org/10.1038/NGEO2365.
Oster, J.L., Weisman, I.E., Sharp, W.D., 2020. Multi-proxy stalagmite records from northern California reveal dynamic patterns of regional hydroclimate over the last glacial cycle. Quat. Sci. Rev. 241, 106411 https://doi.org/10.1016/j.quascirev.2020.106411.
Outcalt, S.I., MacPhail, D.D., 1965. A survey of neoglaciation in the Front Range of Colorado. Univ. Colorado Stud. Earth Sci. 4, 124.
Oviatt, C.G., 1977. Glacial Geology of the Lake Marie area, Medicine Bow Mountains, Wyoming. Contrib. Geol. Univ. Wyo. 16, 27–38.
Palacios, D., Stokes, C.R., Phillips, F.M., Clague, J.J., Alcalá-Reygosa, J., Andres, N., Angel, I., Blard, P.H., Briner, J.P., Hall, B.L., Dahms, D., Hein, A.S., Jomelli, V., Mark, B.G., Martini, M.A., Moreno, P., Riedel, J., Sagredo, E., Stansell, N.D., Vázquez-Selem, L., Vuille, M., Ward, D.J., 2020. The deglaciation of the Americas during the Last Glacial Termination. Earth Sci. Rev. 203, 1–58. https://doi.org/10.1016/j.earscirev.2020.103113, 103113.
Plummer, M.A., Phillips, F.M., 2003. A 2-D numerical model of snow/ice energy balance and ice flow for paleoclimatic interpretation of glacial geomorphic features. Quat. Sci. Rev. 22, 1389–1406. https://doi.org/10.1016/SO277-3791(03)00081-7.
Pribyl, P., Shuman, B.N., 2014. A computational approach to Quaternary lake-level reconstruction applied in the central Rocky Mountains, Wyoming, USA. Quat. Res. 82, 249–259. https://doi.org/10.1016/j.yqres.2014.01.012.
Quirk, B.J., Moore, J.R., Laabs, B.J., Caffee, M.W., Plummer, M.A., 2018. Termination II, Last Glacial Maximum, and Lateglacial chronologies and paleoclimate from Big Cottonwood Canyon, Wasatch Mountains, Utah. Geol. Soc. Am. Bull. 130, 1889–1902. https://doi.org/10.1030/B31967.1.

Quirk, B.J., Moore, J.R., Laabs, B.J., Plummer, M.A., Caffee, M.W., 2020. Latest Pleistocene glacial and climate history of the Wasatch Range, Utah. Quat. Sci. Rev. 238, 1–17. https://doi.org/10.1016/j.quascirev.2020.106313, 106313.

Quirk, B.J., Huss, E., Laabs, B.J.C., Leonard, E., Licciardi, J., Plummer, M.A., Caffee, M. W., 2022. Late Pleistocene glacial chronologies and paleoclimate in the northern Rocky Mountains. Clim. Past 18, 293–312. https://doi.org/10.5194/cp-18-293-2022.

Ray, L.L., 1940. Glacial chronology of the southern Rocky Mountains. Geol. Soc. Am. Bull. 51, 1851–1917.

Refsnider, K.A., Laabs, B.J.C., Plummer, M.A., Mickelson, D.M., Singer, B.S., Caffee, M. W., 2008. Last Glacial Maximum climate inferences from cosmogenic dating and glacier modeling of the western Uinta ice field, Uinta Mountains, Utah. Quat. Res. 69, 130–144. https://doi.org/10.1016/j.yqres.2007.10.014.

Refsnider, K.A., Brugger, K.A., Leonard, E.M., McCalpin, J.P., Armstrong, P.P., 2009. Last glacial maximum equilibrium-line altitude trends and precipitation patterns in the Sangre de Cristo Mountains, southern Colorado, USA. Boreas 38, 663–678. https://doi.org/10.1111/j.1502-3885.2009.00097.x.

Roe, G.H., 2011. What do glaciers tell us about climate variability and climate change? J. Glaciol. 57, 567–578. https://doi.org/10.3189/002214311796905640.

Schaefer, J.M., Denton, G.H., Barrell, D.J., Ivy-Ochs, S., Kubik, P.W., Andersen, B., Phillips, F.M., Lowell, T.V., Schlüchter, C., 2006. Near-synchronous interhemispheric termination of the last glacial maximum in mid-latitudes. Science 312, 1510–1513. https://doi.org/10.1126/science.1122872.

Schweinsberg, A.D., Briner, J.P., Shroba, R.R., Licciardi, J.M., Leonard, E.M., Brugger, K. A., Russell, C.M., 2016. Pinedale glacial history of the upper Arkansas River valley: New moraine chronologies, modeling results, and geologic mapping. In: Keller, S.M., Morgan, M.L. (Eds.), Unfolding the Geology of the West, vol. 44. Geological Society of America Field Guide, pp. 335–353. https://doi.org/10.1130/2016.0044(14.

Schweinsberg, A.D., Briner, J.P., Licciardi, J.M., Shroba, R.R., Leonard, E.M., 2020. Cosmogenic ^{10}Be exposure dating of Bull Lake and Pinedale glaciations and deglaciation in the upper Arkansas River valley, Colorado Rocky Mountains. U.S.A. Quat. Res. 97 https://doi.org/10.1017/qua.2020.21.

Shakun, J.D., Clark, P.U., He, F., Lifton, N.A., Liu, Z., Otto-Bliesner, B.L., 2015. Regional and global forcing of glacier retreat during the last deglaciation. Nat. Commun. 6, 8059. https://doi.org/10.1038/ncomms9059.

Sharma, P., Bourgeois, M., Elmore, D., Granger, D., Lipschutz, M.E., Ma, X., Miller, T., Mueller, K., Rickey, F., Simms, P., Vogt, S., 2000. PRIME lab AMS performance, upgrades and research applications. Nucl. Instrum. Methods Phys. Res. Sect. B Beam Interact. Mater. Atoms 172, 112–123. https://doi.org/10.1016/S0168-583X(00)00132-4.

Shuman, B.N., Serravezza, M., 2017. Patterns of hydroclimatic change in the Rocky Mountains and surrounding regions since the last glacial maximum. Quat. Sci. Rev. 173, 58–77. https://doi.org/10.1016/j.quascirev.2017.08.012.

Sommerfeld, R.A., 1994. Snow. In: Musselman, R.C, 1994. In: The Glacier Lakes Ecosystem Experiments Site (GLEES): an Alpine Global Change Research Study Area. Gen. Tech. Report RM -249. U.S. Department of Agriculture, Forest Service, Fort Collins, CO, pp. 58–59.

Stuiver, M., Reimer, P.J., Reimer, R., 2021. CALIB Manual. http://calib.org/calib/manual/chapter4.html.

Sutherland, W.M., Hausel, W.D., 2004. Preliminary Geologic Map of the Saratoga 30' X 60' Quadrangle, Carbon and Albany Counties, Wyoming. Wyoming State Geological Survey Open File Report 04-10. version 1.1, vol. 36, 1 pl., scale 1:100,000.

Sutherland, W.M., Durnan, J.A., Johnson, J.F., 2013. Preliminary geologic map of the Centennial Quadrangle, Albany County, Wyoming. Wyoming State Geol. Surv. Open File Rep. 13–5 scale 1:24,000.

Thompson, R.S., Whitlock, C., Bartlein, P.J., Harrison, S.P., Spaulding, W.G., Wright, H. E., Kutzbach, J.E., Webb, T.I.I.I., Ruddiman, W.F., Street-Perrott, F.A., 1993. Climatic changes in the western United States since 18,000 yr BP. In: Wright, H.E. (Ed.), Global Climates since the Last Glacial Maximum, pp. 468–513.

Tierney, J.E., Poulsen, C.J., Montañez, I.P., Bhattacharya, T., Feng, R., Ford, H.L., Hönisch, B., Inglis, G.N., Petersen, S.V., Sagoo, N., Tabor, C.R., Thirumalai, K., Zhu, J., Burls, N.J., Foster, G.L., Goddéris, Y., Huber, B.T., Ivany, L.C., Turner, S.K., Lunt, D.J., McElwain, J.C., Mills, B.J.W., Otto-Bliesner, B.L., Ridgwell, A., Zhang, Y. G., 2020. Past climates inform our future. Science 370, 680. https://doi.org/10.1126/science.aay3701.

Tulenko, J.P., Caffee, W., Schweinsberg, A.D., Briner, J.P., Leonard, E.M., 2020. Delayed and rapid deglaciation of alpine valleys in the Sawatch Range, southern Rocky Mountains, USA. Geochronology 2, 1–11. https://doi.org/10.5194/gchron-2-245-2020.

Ward, D.W., Anderson, R.S., Briner, J.P., Guido, Z.S., 2009. Numerical modeling of cosmogenic deglaciation records, Front Range and San Juan mountains, Colorado. J. Geophy. Res.–Earth Surf. 114, F01026 https://doi.org/10.1029/2008JF001057.

Wittke, S.J., Worman, B.N., 2012. Preliminary surficial geologic map of the Centennial Quadrangle, Albany County, Wyoming. Wyoming State Geol. Surv. Open File Rep. 12–4, scale 1:24,000.

Young, N.E., Briner, J.P., Leonard, E.M., Licciardi, J.M., Lee, K., 2011. Assessing climatic and non-climatic forcing of Pinedale glaciation and deglaciation in the western United States. Geology 39, 171–174. https://doi.org/10.1130/G31527.1.

Young, N.E., Briner, J.P., Schaefer, J., Zimmerman, S., Finkel, R.C., 2019. Early Younger Dryas glacier culmination in southern Alaska: Implications for North Atlantic climate change during the last deglaciation. Geology 47, 550–554. https://doi.org/10.1130/G46058.1.